UNIVERSITY OF OKLAHOMA

GRADUATE COLLEGE

STUDY OF ELECTROSPINNING SYNTHESIS PARAMETERS AND VALIDATION OF A POLARIZED SPATIAL FREQUENCY DOMAIN IMAGING DEVICE USING ELECTROSPUN POLYCAPROLACTONE FIBERS AND SCANNING ELECTRON MICROSCOPY

A THESIS

SUBMITTED TO THE GRADUATE FACULTY

in partial fulfillment of the requirements for the

Degree of

MASTER OF SCIENCE

By

LAUNY M. OHANINA
Norman, Oklahoma
2022

STUDY OF ELECTROSPINNING SYNTHESIS PARAMETERS AND VALIDATION OF A POLARIZED SPATIAL FREQUENCY DOMAIN IMAGING DEVICE USING ELECTROSPUN POLYCAPROLACTONE FIBERS AND SCANNING ELECTRON MICROSCOPY

A THESIS APPROVED FOR THE DEPARTMENT OF ENGINEERING PHYSICS

BY

Dr. Chung-Hao Lee, Chair

Dr. Michael Santos

Dr. Preston Larson

Acknowledgments

I will start by extending my thanks and appreciation to my advisor Dr. Chung-Hao Lee for allowing me to do my master's thesis as a member of the Biomechanics and Biomaterials Design Laboratory (BBDL). This truly has been a better experience than what I could have had ever hoped for.

I would also like to thank my other thesis committee members Dr. Michael Santos and Dr. Preston Larson for their consideration of my thesis, and the advice they have provided me along the way. I am grateful for the teachings they have provided me during these past 17 months.

I am also deeply thankful for Sergio Pineda-Castillo without whom none of this would have been possible. He has helped me hugely in the realization of this thesis but also regarding research in general as it was something totally new for me.

I would also like to thank my teachers and the administration at Polytech Clermont-Ferrand in France for helping me apply for the dual degree that allowed me to come to the University of Oklahoma.

My greatest thanks go out to my parents, my family, and my friends for supporting me every step of the way as I was navigating graduate college in a foreign country.

Thank you,

Launy M. Ohanina

Abstract and Keywords

Scaffolds made with electrospun nanofibers are used for many applications in which mechanical properties increase with decreasing the diameter and aligning the fibers. This thesis research investigates the effects of several parameters on the diameter and orientation of fibers fabricated with our custom electrospinning device. Data are collected with SEM and pSFDI with the intent to validate pSFDI as a rapid and non-destructive method of study for microstructures. Experiments showed that a decrease in concentration, increase in tip-collector distance and in flow rate, all reduce the fiber diameter, while an increase in concentration and in flow rate, improve their alignment. The implementation of an auxiliary electrode further improved the alignment of fibers. However, as the results were not optimal and reproducible, many other parameters could be taken into account to obtain highly satisfactory scaffolds. The findings also support the use of pSFDI, but with some limitations.

Keywords: Electrospinning, Fiber Diameter, Fiber Orientation, Polarization Imaging, Scanning Electron Microscopy

Table of Contents

Table of Figures

Table of Tables

CHAPTER 1 – INTRODUCTION

1.1 Motivation

Electrospinning is a process that can be used to produce various types of nanofibers with applications in many fields, such as textiles, cosmetics, medicine, and electrochemical engineering [1, 3]. This experimental technique has been considered as one of the most widely used methods for producing nanofibers and in the last decade, the number of researchers working on it has been increasing significantly [4]. Biodegradable polymer scaffolds can be used as a cell delivery system [5], for the fabrication of nerve conduits and thus improve nerve regeneration [6, 7], for heart valve tissue engineering [8], or more generally for reconstructive and transplantation surgery [5].

If for some applications the fibers can be patterned, the alignment of fibers is generally sought to encourage contact guidance or mechanical properties [8]. Studies have also shown that each application requires a specific fiber size. For instance, to engineer bone tissue, microfibers are preferred over nanofibers, whereas cells were shown to perform better on nanofibers for skin and vascular tissue engineering [6].

However, electrospun materials are sometimes limited because of their lack of reproducibility, which is a major barrier to their widespread utilization. Therefore, being able to control the parameters during the electrospinning process would enable researchers to make scaffolds having aligned fibers with a specific diameter [9], thus resembling an extracellular matrix of biological systems such as collagen fibers [10, 11].

Furthermore, because our group (Biomechanics and Biomaterials Design Laboratory (BBDL)) is working on the cardiac heart valves, we are interested in collagen fibers. Many soft tissue structures and mechanical properties depend on collagen fibers, but current techniques to

quantify their organization are limited by the inability to employ non-contacting, non-modifying, near-real-time fiber imaging [12]. With polarized spatial frequency domain imaging (pSFDI), a novel large-field reflectance-based imaging system, researchers can rapidly assess the preferred fiber orientation on soft collagenous tissues by combining polarized light imaging (PLI) and spatial frequency domain imaging (SFDI) [13].

By scanning the surface of soft tissues over large fields-of-view and measuring the planar collagen fiber orientation, pSFDI can be used to assess fiber architecture in samples at multiple time points, ultimately enabling the study of dynamic fiber structure during active tissue deformation [12].

Because electrospun fibers can be made similar to collagen fibers, being able to use pSFDI as an accurate way to quantify the orientation of electrospun fibers will enable researchers to use pSFDI as an accurate way to understand mechanics and collagen microstructures in live tissues.

Also, pSFDI would help knowing that scaffolds have aligned fibers without using scanning electron microscopy (SEM). Indeed, it would enable the use of the same scaffold for cell culture/tissue regeneration for instance, instead of destroying it with SEM.

1.2 Objectives and Scope

The objectives of this thesis research are to find the electrospinning process parameters that will give us electrospun scaffolds with fibers as aligned as possible with our custom electrospinning device and to verify that pSFDI is able to determine fiber alignment.

For the research on how to improve the fiber alignment, the studies performed involve:

(1) *Understanding the parameters that control the architecture and alignment of fibers*

In this study, trials and errors were made to determine the parameters that influence the architecture of the fibers, in particular their diameter, and fiber orientation. Scaffolds were made with different solution recipes, at several rotational speeds of the collector, with several solution viscosity levels, with several extrusion rates from the syringe, and with several Tip-Collector Distances. Then the scaffolds were analyzed with pSFDI and/or SEM, and the diameter of the fibers was quantified.

(2) *Understanding how to control the fiber alignment*

In this study, trials and errors were made to determine what could be done to improve the alignment of the fibers. Scaffolds were made at several rotational speeds of the collector, with several solution viscosity levels, and with several extrusion rate from the syringe. Then these scaffolds were analyzed with pSFDI and/or SEM, and the alignment of the fibers was quantified.

For the research on how verifying that pSFDI is capable to determine the fiber alignment, the study performed involves:

C*omparing the data obtained with pSFDI and those obtained with the SEM*

In this study, scaffolds were imaged with the SEM and the alignment of the fibers was quantified, then the data were compared to what we obtained with pSFDI.

The remainder of this thesis is organized as follows. Chapter 2 provides a literature review on electrospinning and pSFDI. In Chapter 3, the study to find the parameters that control the fiber architecture and fiber alignment is described. Chapter 4 describes the study on controlling the alignment of the fibers by (i) trying different polymer solution recipes, different viscosities, flow rates, and speeds of the collector, and (ii) implementing an auxiliary electrode to focus the electrospun jet towards the collector. Once our custom electrospinning device was improved, studies on (i) how to improve further the fiber alignment, and (ii) the validation of our pSFDI device are presented in Chapter 5. Chapter 6 concludes this thesis, alongside suggestions for future extensions based upon the work herein.

CHAPTER 2 – LITERATURE REVIEW

2.1 Overview of Electrospinning

2.1.1 Principle

Electrospinning is a technique to produce small quantities of nanofibers using electric forces [4, 14]. It involves a liquid droplet being charged and distorted into a conical shape known as the Taylor cone from which a jet will emerge and be stretched then elongated to generate nanofibers whose average diameter is in between 100 nm and 5600 nm [1, 10, 15]. The basic setup consists of a high-voltage power supply, a programmable syringe pump, a spinneret (commonly a hypodermic needle on a syringe), and a grounded collector (**Figure 2-1**). The collector can be a flat surface, a ring, one or multiple wires, or a rotating mandrel for example [1]. Moreover, the two most common setups are horizontal and top-down (vertical), with different applications. Specifically, in the limited literature we learn that the choice of setup often depends on the materials available and the importance given to the effect of gravity. Indeed, some consider that the effect of gravity is negligible compared to the effect of the electric field [35].

A polymer solution is placed in a syringe to be dispensed by the pump through the charged spinneret. At the tip of the needle, the electrostatic repulsion counteracts the surface tension of the droplets that then form a Taylor cone before being ejected as a jet. As it is stretched through the air, the solvent evaporates, then the jet thins and solidifies, resulting in a fiber that will be deposited on the collector. Whether it's experimentally or theoretically, characterization of the electrospinning process is not an easy task. Several parameters of the electrospinning process, such as solution properties, voltage, distance needle tip to collector and extrusion rate, influence the overall fiber properties [1, 16, 17].

2.1.2 Formation of a Taylor Cone and Stretching of the Jet

Electrostatic repulsion between the surface charges and the Coulombic force due to the applied electric field are the two major types of electrostatic forces that will distort a liquid droplet of solution. The Taylor cone is where the electrostatic repulsion is at an equilibrium with the surface tension. To transform a liquid droplet into a Taylor cone, a critical electric potential (V_C) needs to be reached. V_C can be calculated using **Equation 2.1**:

$$V_C{}^2 = \frac{4H^2}{h^2}\left(\ln\left(\frac{2h}{R}\right) - 1.5\right)(1.3\pi R\gamma)(0.09) \qquad (2.1)$$

where H is the distance between the tip of the needle and the collector in cm, h is the length of the needle in cm, R is the outer radius of the needle in cm, γ is the liquid surface tension in dyn/cm, and V_C is the voltage in kV. The factor 1.3 is derived from $2\cos(49.3)$ when considering that the cone has a semi vertical angle of 49.3°, close to a possible equilibrium value.

After this critical voltage has been reached, a jet is emitted from the cone and accelerated in the direction of the electric field before undergoing a whipping process. As illustrated in **Figure 2-2**, the jet is straight at first for a short period, then the whipping process begins and the jet thins. While the jet goes in a straight line, it's acceleration is progressively decreased because of the viscoelastic force and surface tension that prevent it from moving forward. As a result, the jet starts to stretch until the acceleration becomes a constant or zero and instabilities can affect the jet. [1, 15].

2.1.3 Thinning and Solidification of the Jet

Due to the Coulomb forces resulting from the electrostatic repulsion among surface charges, the electrified jet will bend with what is called bending or whipping instabilities. During the whipping, the solvent starts to evaporate, and the jet thins from hundreds of micrometers to

possibly tens of nanometers and bends by an angle of about 90° into loops that will form a coil around the emission axis. The larger the loops are, the thinner and longer the fiber will be. This process will happen until the surface charge density decreases enough to be balanced by the surface tension. The generated fiber is at that point considered stable and has reached its terminal diameter. The last step of the electrospinning technique is the deposition of the fiber on the collector. Ideally, just before the jet reaches the collector, the solvent will have evaporated due to its movement through the air or other environment [1, 15].

2.1.4 Control of the Electrospinning Process

The formation of fibers, the control of their alignment, and the control of their diameter are directly linked to the choices made regarding the processing parameters. There are lots of them but generally, the first parameters changed are the applied voltage, the concentration of the liquid solution, the flow rate at which is emitted the solution, and the distance between the tip of the spinneret and the collector. Some of those parameters will also impact the shape of the electrospun fibers. Specifically, fibers can be branched, flat, form ribbons or tubes for instance.

Regarding the concentration in polymer, if the solution is too viscous, the fiber motion into loops seen in **Section 2.1.3** will be difficultly realized and the jet will follow a straighter path, thus producing more aligned fibers. However, at a certain limit, the fibers may bend where it is not supposed to. On the contrary, if the solution is not viscous enough, the jet will stay into droplets and the electrospinning process cannot happen.

The working distance, also called collection distance or tip-collector distance (TCD), determines the amount of whipping instability that will have time to happen before the jet is deposited on the collector. If the TCD is too short, the solvent may not have time to evaporate,

therefore the fibers will not solidify and as a result, they will stick to each other on the collector. If the evaporation is able to be done, the fibers will generally be larger than if the distance was longer.

The flow rate as a direct link to the diameter of the fibers and their alignment. Specifically, an increase in flow rate will generally produce more aligned fibers, because of the decrease in whipping instabilities, with a larger diameter. However, if the flow rate is too high, droplets of solution will drip and on the produced fibers beads may be observed. On the contrary, if the flow rate is too low, it may cause a Rayleigh instability that will lead to non-continuous fibers as the jet will breakup into droplets. The Taylor cone may also disappear and on the collector, beads can also be observed. A way to avoid this instability is to create a stronger electric field.

Regarding the voltage, if it is too low, the previously mentioned phenomenon may happen, but if it is too high, the whipping process will start after a longer straight path and the fibers will not have time to solidify, resulting in only liquid jet deposited on the collector.

To control the architecture and alignment of fibers, the processing parameters need to be chosen carefully and optimized. Different choices will produce completely different results in fiber diameter and alignment. Moreover, other parameters such as the temperature or the humidity around the electrospinning device can have important impact on the resulting fibers [1, 6, 14, 15, 18-20].

2.2 Overview of pSFDI

2.2.1 Principle

Polarized spatial frequency domain imaging (pSFDI) is a wide-field reflectance imaging technique based on polarized light scattering from cylindrical particles such as collagen fibers or electrospun polymer fibers [12]. It combines polarized light imaging (PLI) and spatial frequency domain imaging (SFDI) to quickly quantify the orientation of fibers (θ_{fiber}) on soft collagenous tissues or electrospun scaffolds [13]. SFDI is used to control the imaging depth and the images generated are called AC images because they capture the spatially alternating reflected intensities. This will enable pSFDI to produce spatial maps with information only concerning a determined imaging depth [21].

2.2.2 Our pSFDI Device

An integrated pSFDI-biaxial testing system (**Figure 2-3**) was developed at the Biomechanics and Biomaterials Design Laboratory (BBDL), which is the laboratory where this master's thesis research was performed.

The system consists of a pSFDI device vertically placed above a biaxial mechanical tester (BioTester, CellScale, Canada).

The pSFDI devices utilizes:

- a LED projector which projects the incident spatial frequency light patterns with a wavelength of 490 nm (cyan)
- an iris (ID36/M, Thorlabs Inc., USA) to control the amount of incident light from the projector

- a rotation linear polarizer (PR M1/MZ8, Thorlabs Inc., USA) with 37 distinct polarization states (i.e., 0° to 180°, 5° increments)
- a brushed motor controller (KDC101, Thorlabs Inc., USA) linked to the polarizer
- a CCD camera (CS505MU, Thorlabs Inc., USA) which is used to capture the reflected light intensity
- a zoom lens (zoom 7000, Navitar, Japan) linked to the camera
- two dielectric mirrors (400-750 nm) (CCM1-E02/M, Thorlabs Inc., USA) because the sample is not in the direct line of sight of the projector and the camera.

A sample mounted on a biaxial mechanical tester is imaged via the camera capturing the intensity response from the light that is backscattered though the rotating linear polarizer. The incident light coming from the LED projector has a specific spatial frequency that will be shown as a specific pattern of stripes that will, with the polarizer, enable us to obtain the orientation of the fibers. Indeed, the pSFDI imaging technique relies on the birefringent optical response of the fibers. The birefringence is the refractive response depending on the polarization and the propagation of the incident light. For collagen fibers or our electrospun fibers, their cylindrical shape entails a structural birefringence. The backscattered intensity response is captures from 0° to 180° at a 5° increment, resulting in thirty-seven different images of polarization states. Therefore, both the incident light and the reflected light pass through the polarizer with an angle $\theta_{polarizer}$. Because of the specific light pattern projected, the same procedure is repeated for the three linear phase shifts (0°, 120°, and 240°) Also, the choice in spatial frequency will produce a different projected pattern that will correspond to a different depth studied. Specifically, the wider the stripes in the pattern are, the deeper the penetration depth is. Each of the 37 images for each state are then analyzed thanks to custom MATLAB (Matrix Laboratory, MathWorks, USA)

scripts. For each pixel, the gray-scale intensity, representing the birefringent reflected intensity associated with each $\theta_{polarizer}$, is quantified from 0 to 255. The bimodal intensity response is periodic over 180° and the global maximum intensity is when $\theta_{polarizer} = \theta_{fiber}$, which means that the polarizer transmission axis is parallel to the fiber orientation angle. There is also a local maximum when $\theta_{polarizer} = \theta_{fiber} \pm 90°$, which means that the polarizer transmission axis is perpendicular to the fiber orientation angle [12, 13, 21, 36].

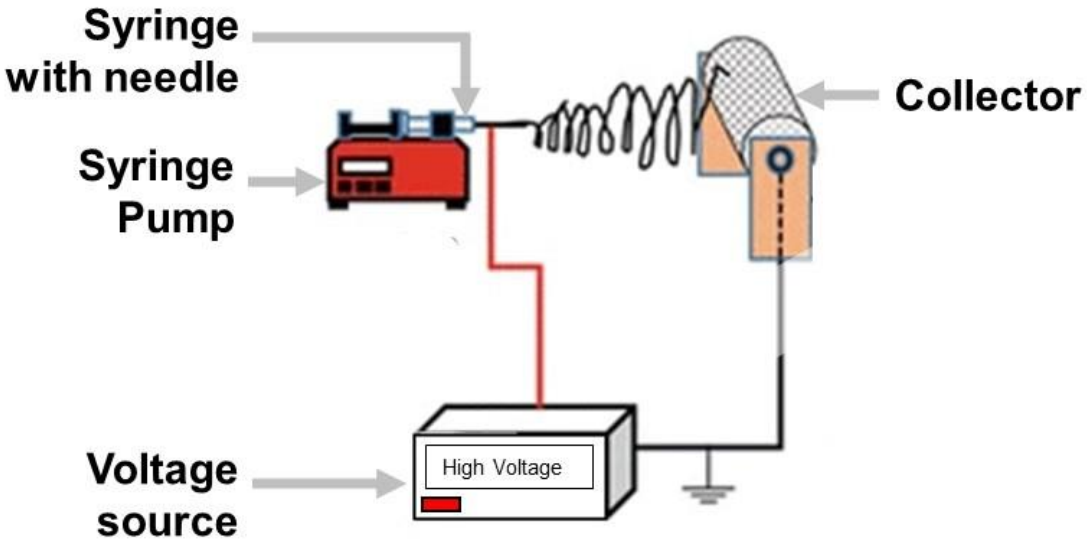

Figure 2-1. Schematic of the electrospinning device [2].

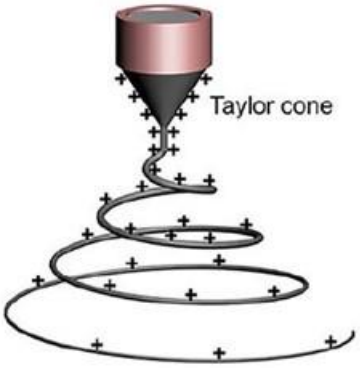

Figure 2-2. Schematic of the whipping process [1].

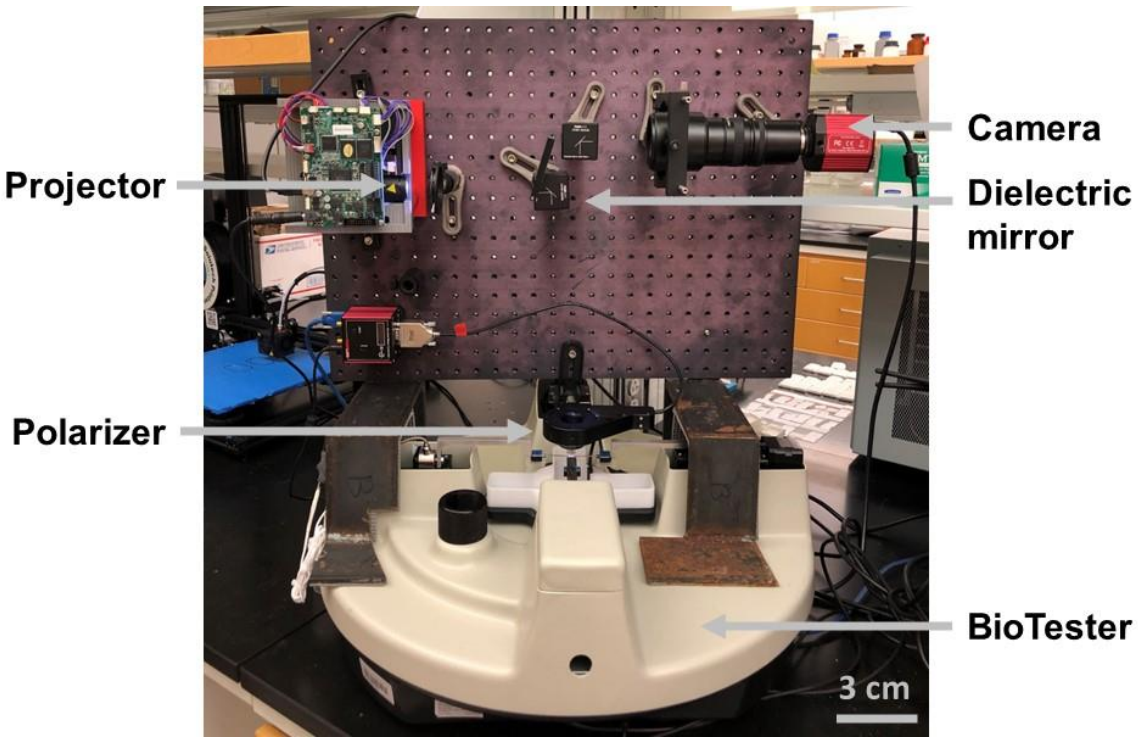

Figure 2-3. Picture of our pSFDI system.

CHAPTER 3 – FIBER ARCHITECTURE CONTROL WITH A CUSTOM ELECTROSPINNING DEVICE

In the previous literature, we have read that some parameters would change the fiber architecture, some would change their orientation, and some would change both [1, 6, 14, 15, 18-20]. However, many of these studies are done with either quite different electrospinning devices from our custom, or with high-tech devices. To advance the knowledge in the fabrication of satisfactory electrospun scaffolds resembling soft collagenous tissues, experiments are warranted to quantify these complex electrospun fibers behaviors.

This chapter summarizes the works pertaining to characterize the architecture of the electrospun fibers with our original electrospinning device. Specifically, the study was about the effects of different electrospinning parameters on the fiber diameters. The remaining of this chapter is organized as follows. The procedures to make the electrospun scaffolds and analyze them are described in Section 3.1. Section 3.2 presents the results of the different studies. The key findings and the implications of the aforementioned results are provided in Section 3.3.

3.1 Methods

3.1.1 Scaffold Fabrication

All scaffolds were made following the Electrospinning Protocol given in **Appendix B**, using a custom electrospinning device. It consists of three major components: (i) a high voltage power supply (20 kV), (ii) a programmable syringe pump, and (iii) a large metallic cylinder (length= 10 cm, radius= 4.5 mm) used as an electrically conductive collector and linked to a motor.

Based on the work of *Bosworth et al.* [22] and *Rabionet et al.* [23], this research for the most affordable ingredients and the fact that Poly(ε-caprolactone) (PCL) has superior rheological and viscoelastic properties as well as a solubility in numerous solvents [6], it was decided to make the scaffolds with Poly(ε-caprolactone) (PCL) and acetone as the biopolymer and non-toxic solvent, respectively. PCL 3 mm pellets with an average molecular weight of 80,000 g/mol (Sigma-Aldrich, USA) were dissolved in acetone (Sigma-Aldrich, USA). Three different concentrations of 5 %w/v, 10 %w/v, and 15 %w/v PCL were achieved. The literature also mentioned that Poly(ethylene oxide) (PEO) would improve the solution elasticity and thus improve the electrospinnability such that enhanced control of the polymer jet for individual nanofiber patterning can be realized [24]. PEO powder with an average molecular weight of 50,000,000 g/mol (Sigma-Aldrich, USA) were dissolved in acetone (Sigma-Aldrich, USA). A concentration of 10 %w/v PCL and 5 %w/v PEO was achieved.

For the PCL+PEO solution, electrospinning was done at 2000 rpm, 3000 rpm, and 4000 rpm, with a flow rate of 7 mL/h and a Tip-Collector Distance (TCD) of 10 cm. For the PCL solution, the scaffolds were made following the parameters shown in **Table 3-1.**

3.1.2 pSFDI Data Acquisition and Analysis

The scaffolds are cylindrical because they are made around a rotating cylindrical collector. Once a scaffold is done, a razor blade is used to cut it from the collector. A rectangular specimen is obtained from which a sample around 1 cm^2 is cut and a dot is placed with a pen in the top right corner so that the long axis being tested is consistent with the longitudinal axis of the mandrel.

The aluminum foil is removed from the sample with tweezers, then the specimen is mounted onto a commercial biaxial mechanical testing system (BioTester, CellScale Biomaterials

Testing, Canada) thanks to four BioRakes (**Figure 3-1**). The effective testing region is 6x6 mm. The sample is then submerged in a 37°C phosphate-buffered saline (PBS) bath to emulate physiological conditions. This step is only to stay coherent with the analysis or soft collagenous tissues.

The detailed procedure for the pSFDI resulting in the imaging of the scaffolds is provide in **Appendix C**.

3.1.3 Scanning Electron Microscopy (SEM) Analysis

(1) *Sample Preparation for SEM*

The sample was placed with tweezers on a stub but because it had to be conductive for the SEM to work, carbon tape was used to stick the sample to the stub. Then the stub was placed in a sputter coater (Hummer VI Plasma Sputter Coater, Anatech LTD, USA) that coated the sample with around 5 nm of Gold Palladium (AuPd) alloy. The reason the sample is coated with a thin metal coating is to increase conductivity and thus reduce charging effects in insulating samples [18].

(2) *Sample Preparation for Environmental SEM (ESEM)*

ESEM allows specimens to be imaged in their natural environment so there is no need for metal coating. The downside is the possible presence of charging artifacts due to the insulating sample charging up under the negatively charged electron beam although the use of the low vacuum mode helps to mitigate these charging artifacts. The sample was simply taped with carbon tape onto the stage (no need for stubs) [18].

(3) *Imaging and Analysis*

PCL fibers were visualized using a scanning electron microscope (Zeiss NEON 40 EsB, Zeiss, Germany) or an Environmental scanning electron microscope (ThermoFisher Quattro S, Thermo Fisher Scientific, USA) and images were captured for further morphological analysis. As for processing, the ImageJ (National Institutes of Health, USA) analysis software was used with the plugins DiameterJ to obtain the distributions of fiber diameter, or the measurements could be done manually. Either way, between 75 and 600 fiber diameters were measured. To obtain the fiber orientation distribution, the plugin OrientationJ was used, but to realize statistical analysis, we used the software Prism (GraphPad, USA).

3.1.4 Statistical Analysis

Statistical analysis was performed in Prism (GraphPad, USA) and fiber diameter results from the SEM experiments were reported as the mean + standard deviation (SD). First, the fiber diameters were compared for three different tip-collector distances, then for three different concentrations of PCL, for three different flow rates, and finally for five different rotational speeds. We tested the normality first, then a “non-parametric” version of one-way analysis variance (ANOVA) for multiple groups of factors test, Kruskal-Wallis test, was performed and it gave us *p*-values that are shown on the graphs with asterisks. Significance probabilities or *p*-values measure the degree of relationship between the data and the hypothesis [25]. A comparison that would produce a p-value < 0.05 was considered as statistically significant, pointing towards consequential variations.

3.2 Results

3.2.1 Results from the PEO Study

A number (*n*) of 75 to 180 fiber diameters were measured for the scaffolds made at three different speeds with PCL + PEO, and for the scaffolds made with pure PCL (**Figure 3-2**). It is obvious that the distributions are similar. Indeed, the fiber diameters were on average more or less the same for each studied sample. For pure PCL, they ranged from 0.222 μm to 25.554 μm with means at 8.444 μm for the scaffold at 2000 rpm (n = 75), 8.332 μm for the scaffold at 3000 rpm (n = 75), and 7.421 μm for the scaffold at 4000 rpm (n = 75). For PCL + PEO, they ranged from 0.889 μm to 34.176 μm with means at 7.991 μm for the scaffold at 2000 rpm (n = 75), 6.494 μm for the scaffold at 3000 rpm (n = 75), and 9.484 μm for the scaffold at 4000 rpm (n = 180).

In addition, SEM images were taken for a sample with PCL + PEO and a sample with pure PCL (**Figure 3-3**). An increase in fiber alignment and in fiber diameter can be noticed when using PEO at high speeds (4000 rpm), however, this increase in diameter is made with the presence of clumps.

3.2.2 Results from the Study on the Effect of TCD on Fiber Diameters

A number n = 500 fiber diameters were measured for each scaffold made with PCL at three different tip-collector distances (TCD) (**Figure 3-4**). The diameters were ranging from 0.047 μm to 9.827 μm with means at 1.578 μm for the scaffold at 5 cm, 0.622 μm for the scaffold at 10 cm, and 0.631 μm for the scaffold at 15 cm. We tested normality but none of the parameters were distributed normally, so we performed Kruskal-Wallis tests that gave us *p*-values. The fiber diameters for the TCD of 10 cm and 15 cm are clearly similar and smaller than the diameters with a TCD of 5 cm. Specifically, the *p*-values for the comparisons were both $p < 0.0001$.

However, with our solution, the TCD of 5 cm and 15 cm were too short and too long respectively because it resulted in unwanted deposition around the collector (see **Section 5.2.1**).

3.2.3 Results from the Study on the effect of Concentration on Fiber Diameters

A number (*n*) of 500 to 600 fiber diameters were measured for each scaffold made with PCL at three different concentrations (**Figure 3-5**). The solution with a concentration of 5 %w/v PCL resulted in fibers that were very thin. Specifically, they ranged from 0.033 μm to 0.960 μm with a mean at 0.199 μm ($n = 600$). The solution with a concentration of 10 %w/v PCL resulted in fibers whose diameters were rather thin but acceptable. Specifically, they ranged from 0.044 μm to 2.383 μm with a mean at 0.542 μm ($n = 500$). And finally, the fiber diameters measured for the solution with a concentration of 15 %w/v PCL were medium to large. Specifically, they ranged from 0.254 μm to 11.037 μm with a mean at 2.468 μm ($n = 550$). We tested normality but none of the parameters were distributed normally, so we performed Kruskal-Wallis tests that gave us *p*-values. For each comparison, we obtained $p < 0.0001$.

However, the solution at 5 %w/v was not viscous enough for a flow rate of 5 mL/h. Small drops were falling from the needle and the scaffolds was made of several clumps.

3.2.4 Results from the Study on the Effect of Flow Rate on Fiber Diameters

A number n = 500 fiber diameters were measured for each scaffold made with PCL at three different flow rates (**Figure 3-6**). While the difference in fiber diameter was minimal between 3 mL/h and 5 mL/h as well as between 5 mL/h and 7 mL/h, it was a little more noticeable between 3 mL/h and 7 mL/h. Specifically, the diameters were ranging from 0.125 μm to 9.827 μm with means at 1.183 μm for the scaffold at 3 mL/h, 0.920 μm for the scaffold at 5 mL/h, and 0.830 μm for the scaffold at 7 mL/h. We tested normality but none of the parameters were distributed

normally, so we performed Kruskal-Wallis tests that gave us *p*-values. The *p*-values for the comparisons of fiber diameters between scaffolds made at 3 mL/h and 5 mL/h, as well as between scaffolds made at 5 mL/h and 7 mL/h, were both $p < 0.05$ (0.011 and 0.048 respectively). For the comparison of fiber diameters between scaffolds made at 3 mL/h and 7 mL/h we obtained $p < 0.0001$.

However, 7 mL/h was a flow rate that was too fast for a solution at 10 %w/v. Small drops were falling from the needle and the scaffolds was made of several clumps.

3.2.5 Results from the Study on the Effect of Rotational Speed on Fiber Diameters

A number (*n*) of 452 to 948 fiber diameters were measured for the scaffolds made with PCL at five different speeds (**Figure 3-7**). Specifically, the diameters were ranging from 0.139 μm to 6.031 μm with a mean at 0.783 μm for the scaffold at 500 rpm ($n = 948$), from 0.124 μm to 9.271 μm with a mean at 1.096 μm for the scaffold at 1000 rpm ($n = 452$), from 0.125 μm to 3.377 μm with a mean at 0.574 μm for the scaffold at 1500 rpm ($n = 500$), from 0.23 μm to 5.408 μm with a mean at 0.936 μm for the scaffold at 2000 rpm ($n = 500$), and from 0.130 μm to 2.615 μm with a mean at 0.731 μm for the scaffold at 2500 rpm ($n = 500$). We tested normality but none of the parameters were distributed normally, so we performed Kruskal-Wallis tests that gave us *p*-values. The values were different but there was no real trend discernible.

3.3 Discussion

3.3.1 Overall Findings from the PEO Study

We found that the distributions of fiber diameter are similar regardless of the adopted solution (**Figure 3-2**) and that many clumps were present with PEO. We thus decided to not pursue

the PEO study at the moment. As viscosity is a factor of fiber alignment [6], the lack in viscosity when using pure PCL can simply be resolved by increasing the concentration of PCL.

3.3.2 Overall Findings from the Study on the Effect of TCD on Fiber Diameters

We also found that the Tip-Collector Distance (TCD) has effects on the deposition time, impacting the solvent evaporation status (dry or wet) when the fibers reach the collector, the TCD can thus significantly influence the fiber diameter. Reducing the TCD leads to an increase of fiber diameter. However, as the TCD also affects the electric field and the whipping motion, the deposition becomes messy along with the undesired deposition of fibers around the collector [4, 6, 15, 20].

Therefore, distances of 5 cm and 15 cm were too short and too long respectively and a TCD of 10 cm was chosen as a fixed parameter moving forward.

3.3.3 Overall Findings from the Study on the Effect of Concentration on Fiber Diameters

This study highlights that the fiber diameter increases with the concentration. Indeed, as a solution at a higher concentration is more viscous, the stretching of the jet is reduced and the fibers become larger. To counteract that phenomenon, the applied electric field would need to be stronger [6].

3.3.4 Overall Findings from the Study on the Effect of Flow Rate on Fiber Diameters

Figure 3-6 shows that for our polymer solution, the fiber diameters seem similar at the three different flow rates. However, the flow rate of 7 mL/h seemed too high because dripping of the solution from the needle tip occurred. This is corroborated by the literature. Indeed, within a certain range, flow rate does not affect fiber diameter but once the flow rate exceeds a certain limit,

the repulsive force due to the charges on the solution is insufficient to draw the solution away from the needle tip and dripping of solution, as well as deposition of fibers that are not dry, happen [19, 20].

3.3.5 Overall Findings from the Study on the Effect of Rotational Speed on Fiber Diameters

As seen in **Figure 3-7**, all speeds present almost the same distribution of fiber diameter. However, even if most of the changes on the diameter of the fibers were happening before they are deposited on the collector (see **Sections 3.3.2** to **3.3.4**), as the rotational speed of the collector increases, the fiber diameter should decrease due to the fact that once deposited on the mandrel, the fibers are pulled along with force at high speed [20].

3.4 Concluding Remarks

In this chapter, studies showed that even if PEO has a positive influence on fiber alignment, the presence of clumps makes it not worth it for the moment as an increase of PCL concentration may work too. Studies also showed that a decrease in concentration, an increase in tip-collector distance, and an increase in flow rate all reduce the fiber diameter. Now that a TCD has been chosen based on fiber diameter, the other parameters need to be further evaluated based on fiber alignment, as will be discussed in the next chapter.

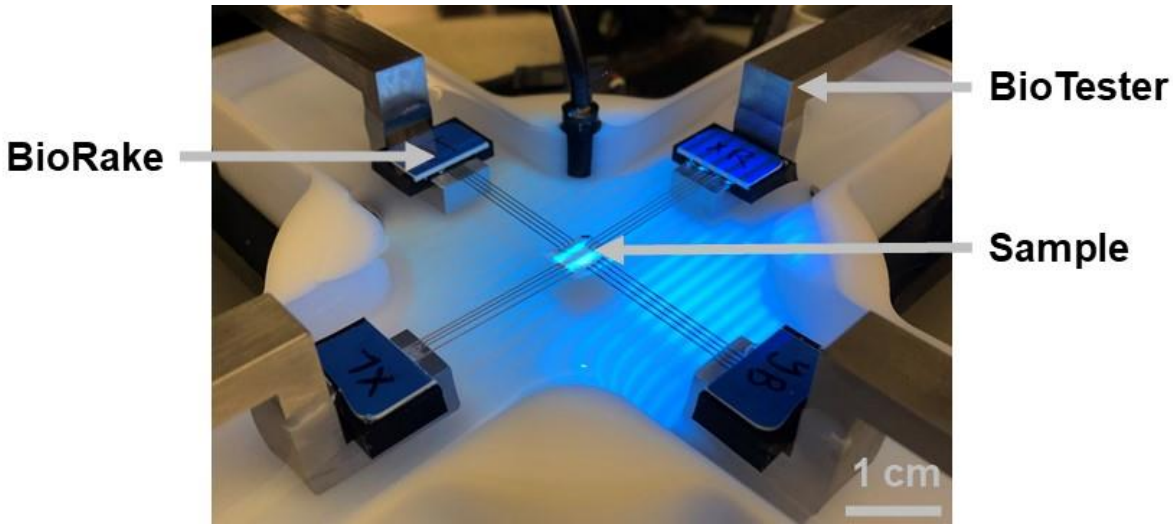

Figure 3-1. Picture of a sample mounted with BioRakes.

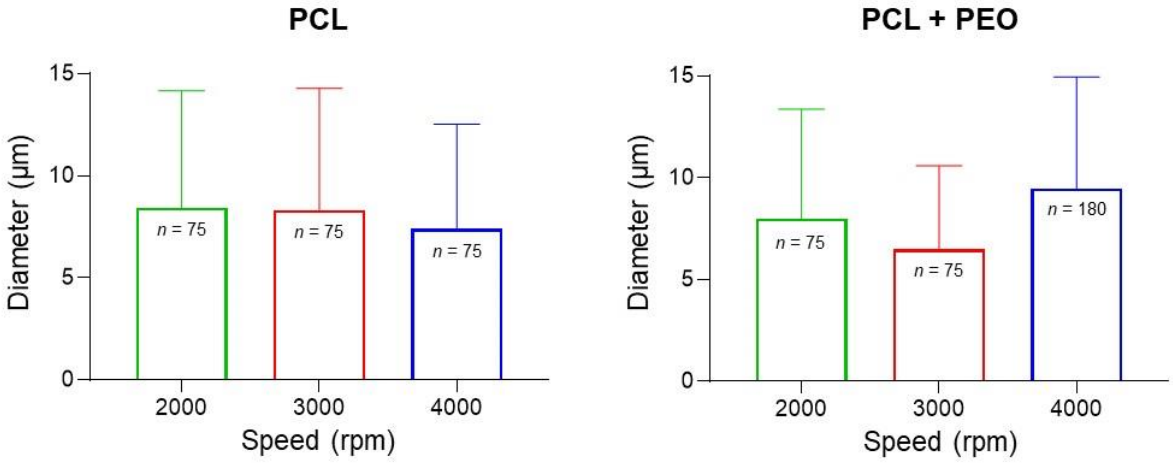

Figure 3-2. Fiber diameter depending on the speed for pure PCL (*left*) and for PCL + PEO (*right*). (Data reported as mean + SD)

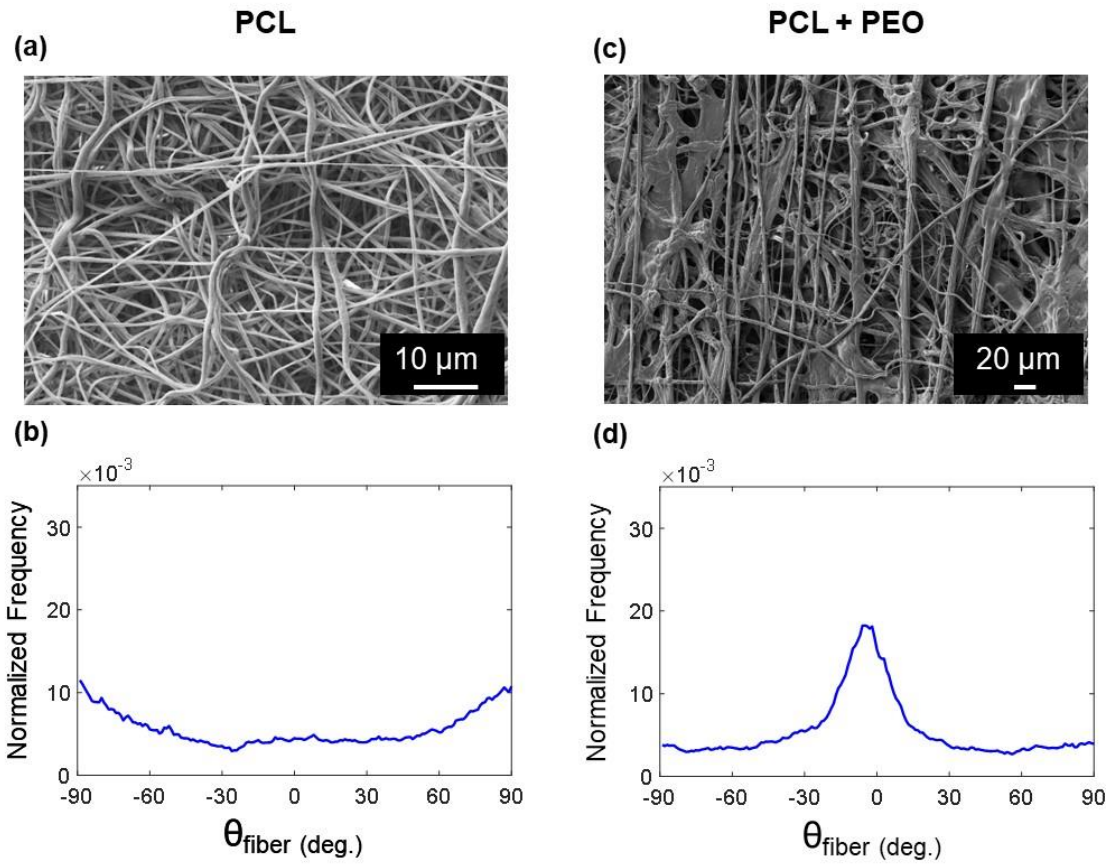

Figure 3-3. (a) SEM image of fibers made from PCL, (b) fiber distribution for PCL, (c) SEM image of fibers made from PCL + PEO, and (d) fiber distribution for PCL + PEO.

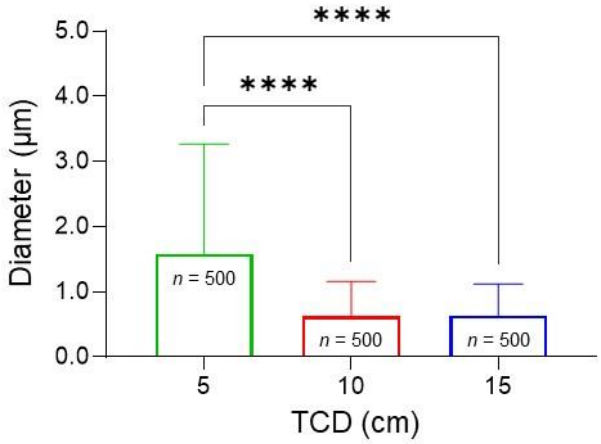

Figure 3-4. Fiber diameter as a function of the TCD. (Data reported as mean + SD and Significance levels: ns: $p > 0.05$, ∗ for $p < 0.05$, ∗∗ for $p < 0.01$, ∗∗∗ for $p < 0.001$, and ∗∗∗∗ for $p < 0.0001$)

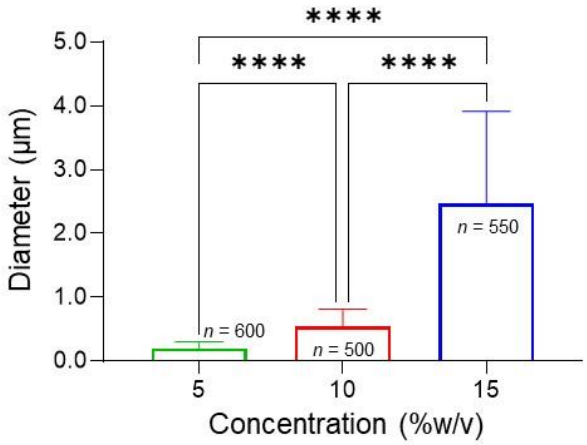

Figure 3-5. Fiber diameter as a function of the concentration of PCL. (Data reported as mean + SD and Significance levels: ns: $p > 0.05$, ∗ for $p < 0.05$, for $p < 0.01$, ∗∗∗ for $p < 0.001$, and ∗∗∗∗ for $p < 0.0001$)

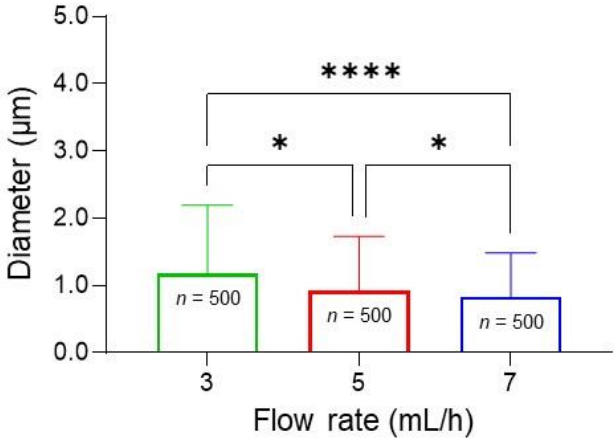

Figure 3-6. Fiber diameter as a function of the flow rate. (Data reported as mean + SD and Significance levels: ns: $p > 0.05$, ∗ for $p < 0.05$, ∗∗ for $p < 0.01$, ∗∗∗ for $p < 0.001$, and ∗∗∗∗ for $p < 0.0001$)

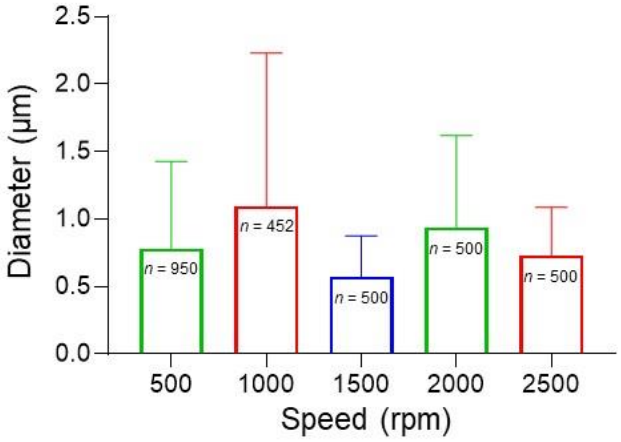

Figure 3-7. Fiber diameter depending on the speed.
(Data reported as mean + SD)

Table 3-1. Parameters for the fabrication of scaffolds to study fiber diameters.

Experiment Tag	Concentration (%w/v)	TCD (cm)	Voltage (kV)	Flow Rate (mL/h)	Dispensed Volume (mL)	Speed (rpm)
PCL_C5	5	10	20	5	2	1000
PCL_C10	10	10	20	5	2	1000
PCL_C15	15	10	20	5	2	1000
PCL_D5	10	5	20	5	2	1000
PCL_D10	10	10	20	5	2	1000
PCL_D15	10	15	20	5	2	1000
PCL_F3	10	10	20	3	2	1000
PCL_F5	10	10	20	5	2	1000
PCL_F7	10	10	20	7	2	1000

CHAPTER 4 – FIBER ALIGNMENT CONTROL WITH A CUSTOM ELECTROSPINNING DEVICE

In the previous chapter, our focus has largely been on finding how some parameters of the electrospinning process would affect the architecture of the fibers so that choices can be made to further study the fiber alignment. Now that some parameters have been fixed, we aim to find the parameters of the electrospinning process to obtain the most aligned fibers with our custom electrospinning device.

Specifically, the Tip-Collector Distance (TCD) has been set to 10 cm, and the study is designated to understand the fiber alignment with varied concentrations, flow rates, and rotational speeds.

This chapter summarizes the works pertaining to improving the alignment of the electrospun fibers and facilitating ways to improve our electrospinning process. Specifically, the studies include: (i) the fabrication of scaffolds with the parameters set by the end of Chapter 3; (ii) the fabrication of scaffolds with a different polymer solution recipe; and (iii) the improvement of our electrospinning device. The remaining of this chapter is organized as follows. The procedures to make the electrospun scaffolds and analyze them, and what has been done to improve the device are described in Section 4.1. Section 4.2 presents the results of these studies, whereas the key findings and the implications are provided in Section 4.3.

4.1 Methods

4.1.1 Scaffolds Fabrication

All scaffolds were made following the Electrospinning Protocol given in **Appendix B**, using our custom electrospinning device.

As in Chapter 3, we fabricated the scaffolds with poly(ε-caprolactone) (PCL) and acetone as biopolymer and non-toxic solvent, respectively: PCL 3 mm pellets with an average molecular weight of 80,000 g/mol (Sigma-Aldrich, USA) were dissolved in acetone (Sigma-Aldrich, USA).

The best concentration has yet to be determined, so two different concentrations of 10 and 15 %w/v PCL were considered.

A solution at 20 %w/v was also investigated with regards to **Section 3.3.1**, but it was found to be much too viscous: even after five hours of dilution, the solution was still not homogeneous.

The objectives here were to choose a concentration, then a flow rate, and finally an optimal rotational speed. Therefore, the scaffolds were made following the parameter sets shown in **Table 4-1**.

Another recipe for the polymer solution was also tested. In the literature, formic acid has been used with PCL to allow for nanofibers with a smaller diameter [26]. Two solutions were made at the following concentrations: 15 %w/v and 20 %w/v.

4.1.2 Polarized Spatial Frequency Domain Imaging (pSFDI) Data Collection and Analysis

As in **Section 3.1.2**, a sample was cut from the scaffold, except that now it was a rectangular sample around 1.5x1 cm. This shape was chosen to be sure that the long axis being tested is consistent with the longitudinal axis of the mandrel.

Also, for some of the scaffolds, the specimen was stretched by the BioTester. The goal was to see if it would change the overall fiber alignment.

4.1.3 Improvement of the Electrospinning Device

The jet of polymer leaving the needle tip was very wide so the research for a way to focus it on the collector led us to designing an auxiliary electrode. Indeed, by reducing the whipping instability, the fibers are deposited in a more aligned way because the auxiliary electrode will direct the electrospun jet [6].

Several articles mentioned the use of a conical-shaped electrode [27, 28], but many others mentioned a cylinder that would be slid on the needle. Different articles mentioned varied sizes of cylinders, so the **Table 4-2** was used to decide on which one to design.

A cylindrical electrode made of aluminum with an inner radius (r) of 13 mm and a thickness (t) of 1 mm was designed with the software SolidWorks (Dassault Systèmes, France) **(Figure 4-1)**. It was then made by the Aerospace and Mechanical Engineering (AME) machine shop. This electrode was insulated with rubber for which a mold was designed, 3D-printed, and implemented **(Figure 4-2)**.

4.2 Results

4.2.1 Results from the Study on the Effect of Concentration on Fiber Alignment

For studying the effect of the solution concentration on fiber alignment, a trend was observed **(Figure 4-3)**. For each speed, knowing that the thinner and higher the peak is, the more accurately *aligned* the fibers are along a specific orientation axis, and the wider and shorter the curve is, the more *randomly* the fibers are deposited and thus the less aligned, we can see that the

scaffolds made with a solution at 15 %w/v PCL were aligned in one strongly predominant direction, whereas those made with a solution at 10 %w/v PCL had fibers more randomly oriented. Furthermore, one main peak can be seen for the solutions at 15 %w/v PCL, while several smaller peaks form the graphs for the solutions at 10 %w/v PCL.

4.2.2 Results from the Study on the Effect of Flow Rate on Fiber Alignment

From the effect of the flow rate on the alignment of the fibers, a trend was also discernible **(Figure 4-4).** For each speed, the scaffolds made with a flow rate of 5 mL/h were aligned in a more *predominant* direction than those made with a flow rate of 3 mL/h that had fibers more *randomly oriented*. It is obvious that the distribution of fibers is more centered for the 5 mL/h flow rate than for the 3 mL/h flow rate. However, the results were not reproducible. The degree of alignment was every time different.

4.2.3 Results from the Study on the Effect of Rotational Speed on Fiber Alignment

Now that every electrospinning parameter was fixed, except for the rotational speed of the collector, the goal was to pinpoint an optimal rotational speed for a polymeric solution. However, a distinct trend could not be observed from this parametric study (**Figure 4-5a**). Specifically, for each speed, the distribution of fibers is similar. If one speed had to be chosen as the best though, it would be 4500 rpm due to the presence of one unique peak, whereas the other distributions contain minor secondary peaks.

In addition, the potential change in fiber distribution with a stretched sample was also examined with these scaffolds. A visual comparison between **Figure 4-5a** and **Figure 4-5b** demonstrates that stretching the sample does not affect the overall fiber alignment results.

4.2.4 Results from the Reproducibility Study

Reproducibility of the results between different scaffolds made with the same parameters, as well as reproducibility of the results within the same scaffold were studied.

Two additional scaffolds were fabricated at a rotational speed of 4500 rpm to see if the result obtained in **Section 4.2.3** was reproducible. In order to maintain consistency, the samples studied with pSFDI were sections of the scaffolds located at the same place, i.e., towards the middle of the scaffolds. **Figure 4-6** displays the fact that the distribution is not the same, thus showing that the results are not perfectly reproducible.

Moreover, when two sections are cut at different places from the same scaffold, the distribution of fibers is also different between the two samples (**Figure 4-7**).

4.2.5 Results from the Formic Acid Study

Two solutions were made by diluting PCL in formic acid (Sigma-Aldrich, USA). The first one was at a concentration of 15 %w/v but the smell was really strong, and it was splashing rather than producing a jet of nano fibers **(Figure 4-8)**. Increasing the viscosity, to fix the second problem, to a concentration of 20 %w/v was then done, but the smell problem was still present. Moreover, the second viscosity was still not allowing the creation of a good jet of fibers.

4.3 Discussion

4.3.1 Overall Findings from the Study on the Effect of Concentration on Fiber Alignment

This study corroborates what can be read in literature. Specifically, the alignment of the fibers is better at higher concentrations of the polymeric solution. The rationale may lie in the fact that, as the concentration increases, the jet's chaotic motion, known as bending instability or

whipping motion, decreases, which leads the jet to follow a straighter path towards the collector and thus produce better aligned fibers [6].

4.3.2 Overall Findings from the Study on the Effect of Flow Rate on Fiber Alignment

The present study conveys what can be read in literature. Indeed, the alignment of the fibers is better when the scaffold is done with a higher flow rate, without reaching the above-mentioned limit (see **Section 3.3.4**).

The rationale may lie in the fact that a higher flow rate entails an increased volume and initial radius of the jet at the tip of the needle, which reduce bending instability that is needed to lead the jet to follow a straighter path towards the collector and thus produce better aligned fibers [6, 19].

However, in this parametric study the reproducibility is not guaranteed because the flow rate is linked to other parameters such as the electric field that we would need to modify along with the flow rate to obtain more reproducible fibers.

4.3.3 Overall Findings from the Study on the Effect of Rotational Speed on Fiber Alignment

Because the reproducibility of results is not ideal (see **Section 4.2.4**) and all the speeds present rather similar distributions (**Figure 4-5a**), pinpointing an optimal speed was not really possible. However, what should have been found is that the best results in terms of alignment occur at the highest speeds because the collector mechanically draws the fibers around it [20, 29].

4.3.4 Overall Findings from the Reproducibility Study

The present study highlights the non-replicability of scaffolds with our current custom electrospinning device. This has been noticed for each scaffold done during this thesis research up to this point. If not for some exceptions, the fibers distribution is different for each scaffold while they were done with the same parameters. As mentioned previously, it is the intricate interplay of several processing parameters that controls the fiber alignment and diameter. However, one solution to improve reproducibility seems to be the one to take care firstly. Indeed, as the whipping instability is a big part of what causes the randomness of alignment of fibers, being able to decrease this instability would help with the reproducibility.

This prompted the research on how to focus the jet of fibers (see **Section 4.1.3**) because the thought was that focusing the fibers to go in a more direct way towards the collector would enable the fabrication of better scaffolds and thus enable reproducibility.

4.3.5 Overall Findings from the Formic Acid Study

This study has provided insights into the fact that the use of different solvents changes radically the electrospinning process. Indeed, the use of formic acid is not as simple as the use of acetone. Moving the electrospinning device under a fume hood could have been done for the smell problem, and an adequate concentration could have been found, but we decided not to further complete this study and focused again on the recipe PCL/acetone.

4.4 Concluding Remarks

In this chapter, the main objective was to find the parameters to obtain the most aligned fibers with our custom electrospinning device. It was found that an increase in concentration and in flow rate help fiber alignment. However, even if conclusions could be drawn from some of the

studies at this time, the overall findings made us consider the fact that accurate results would not be obtained without an improved electrospinning device.

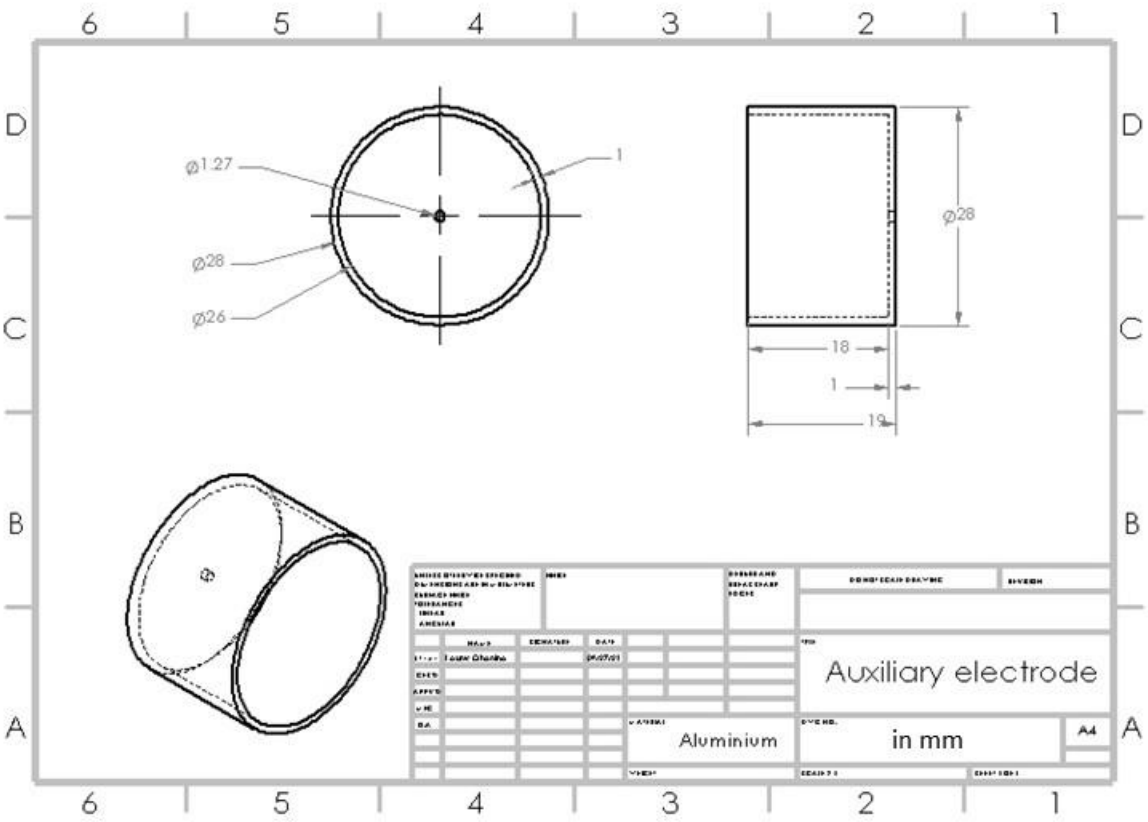

Figure 4-1. SolidWorks drawing of the auxiliary electrode.

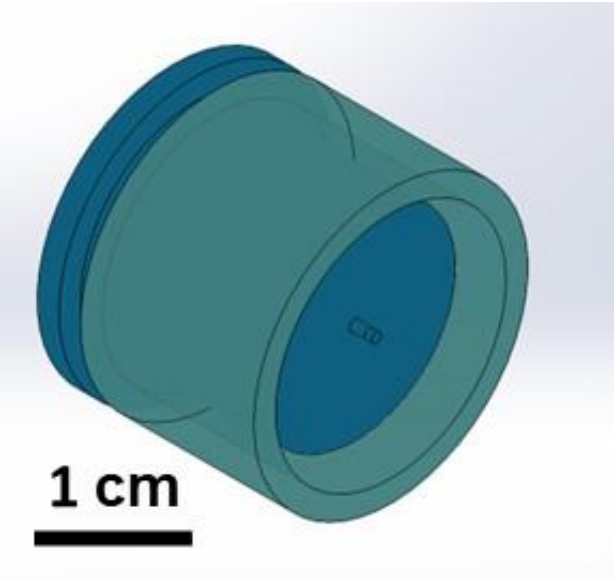

Figure 4-2. SolidWorks mold design for the rubber insulating the auxiliary electrode.

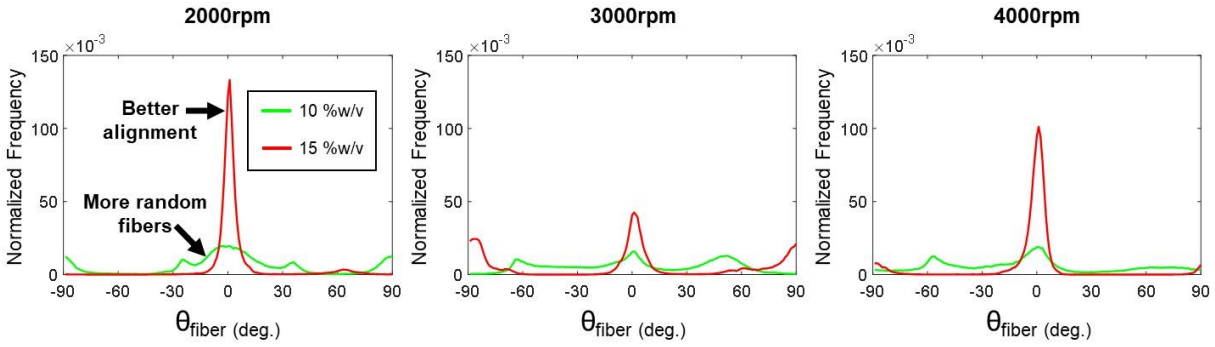

Figure 4-3. Distributions of fibers depending on the concentration, for three different rotational speeds.

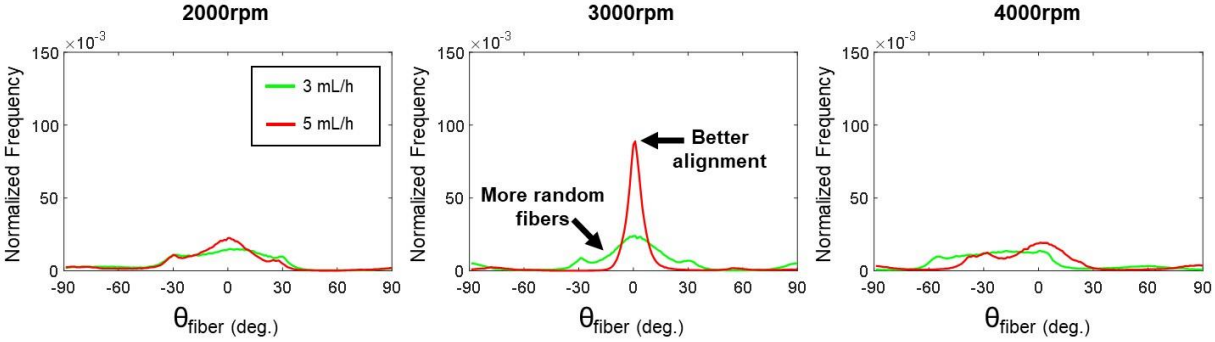

Figure 4-4. Distributions of fibers with varying flow rates, for three different rotational speeds.

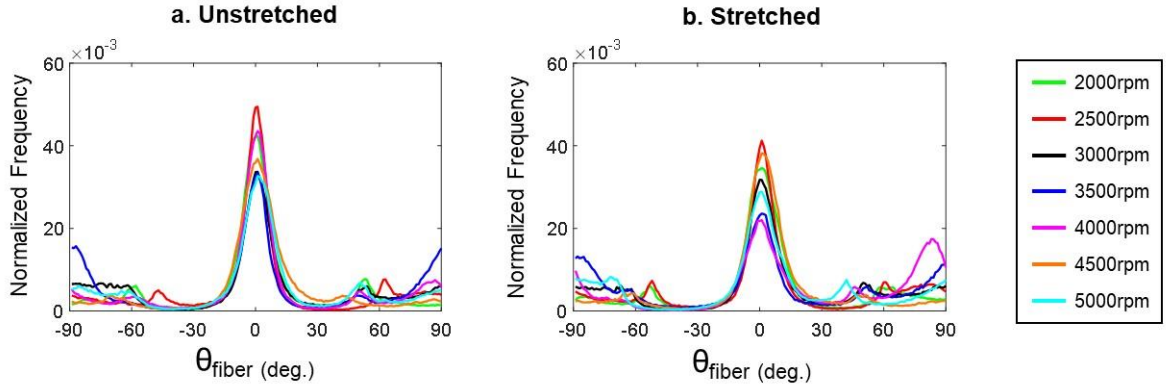

Figure 4-5. Distributions of fibers with varying rotational speeds, for a sample: (a) unstretched and (b) stretched.

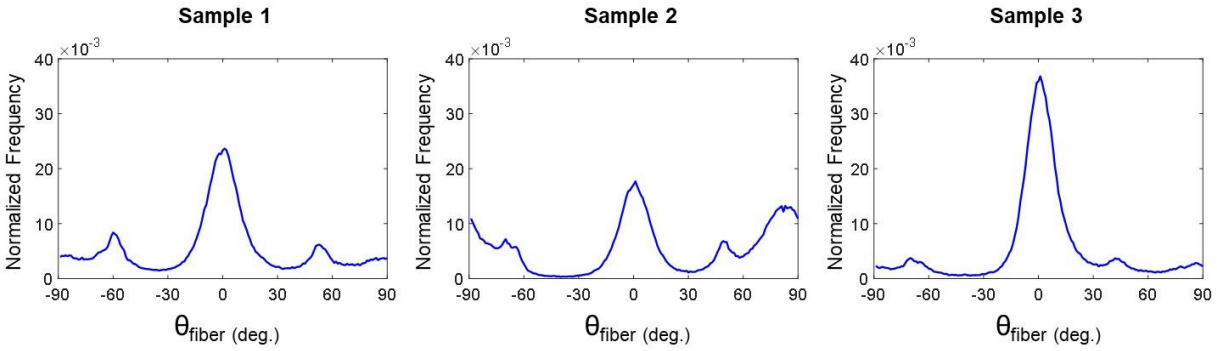

Figure 4-6. Distributions of fibers for three different samples fabricated at 15 %w/v PCL, with a flow rate of 5 mL/h and a rotational speed of 4500 rpm.

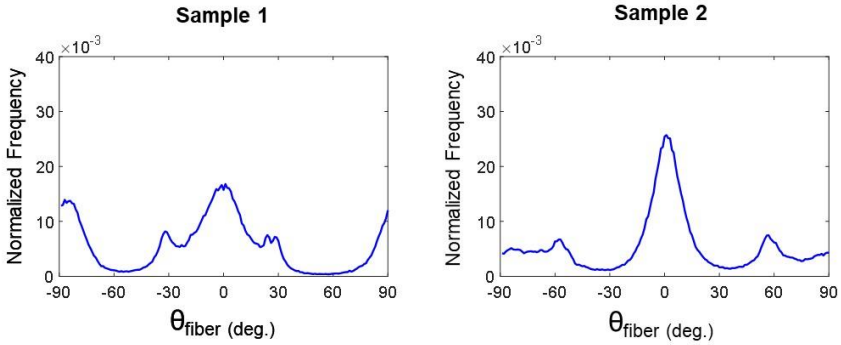

Figure 4-7. Distributions of fibers for two pieces of the same scaffold.

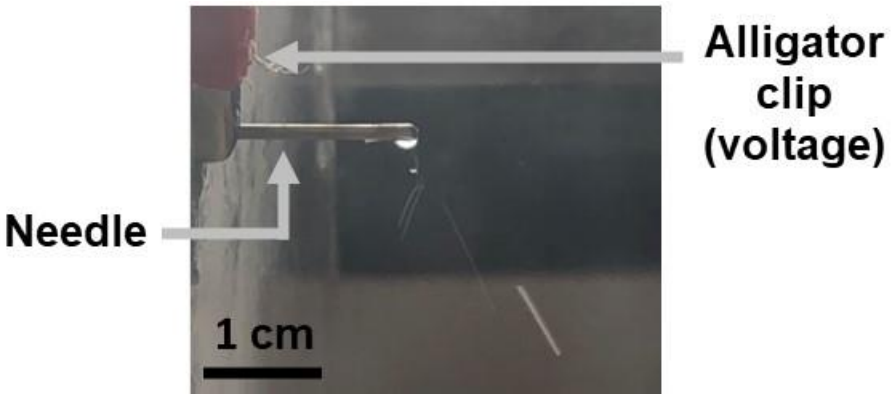

Figure 4-8. Photo showing the splashing of solution at the tip of the needle.

Table 4-1. Parameters for the fabrication of scaffolds to study fiber alignment.

Experiment Tag	Concentration (%w/v)	TCD (cm)	Voltage (kV)	Flow Rate (mL/h)	Dispensed Volume (mL)	Speed (rpm)
PCL_C10_F5_2000rpm	10	10	20	5	2	2000
PCL_C10_F5_3000rpm	10	10	20	5	2	3000
PCL_C10_F5_4000rpm	10	10	20	5	2	4000
PCL_C15_F5_2000rpm	15	10	20	5	2	2000
PCL_C15_F5_3000rpm	15	10	20	5	2	3000
PCL_C15_F5_4000rpm	15	10	20	5	2	4000
PCL_C15_F3_2000rpm	15	10	20	3	2	2000
PCL_C15_F3_3000rpm	15	10	20	3	2	3000
PCL_C15_F3_4000rpm	15	10	20	3	2	4000
PCL_C15_F5_2000rpm	15	10	20	5	2	2000
PCL_C15_F5_2500rpm	15	10	20	5	2	2500
PCL_C15_F5_3000rpm	15	10	20	5	2	3000
PCL_C15_F5_3500rpm	15	10	20	5	2	3500
PCL_C15_F5_4000rpm	15	10	20	5	2	4000
PCL_C15_F5_4500rpm	15	10	20	5	2	4500
PCL_C15_F5_5000rpm	15	10	20	5	2	5000

Table 4-2. Summary of the dimensions used for the auxiliary electrode in each paper.

Dimensions / Papers	*d*=22mm conical	*r*=13mm *t*=1mm	*d*=25mm *l*=30mm *t*=0.4mm	*r*=11mm conical	*d*=22m *l*=20mm	*r*=13mm *t*=0.45mm
Effect of an auxiliary electrode on the crystalline morphology [27]	⊗					
Stability analysis for multi-jets electrospinning process [30]		⊗				
Nanofiber spraying method with a supplementary electrode [31]			⊗			
Electrospun PCL nanofibers with anisotropic mechanical properties [28]				⊗	⊗	
Electrospinning using field-controllable electrodes [32]		⊗				
Highly porous 3D nanofiber scaffold [33]		⊗				⊗

CHAPTER 5 – FIBER ALIGNMENT CONTROL WITH AN IMPROVED CUSTOM ELECTROSPINNING DEVICE AND PRELIMINARY VALIDATION OF PSFDI

In the previous chapter, the determination of the electrospinning parameters that enable the fabrication of scaffolds with the most aligned fibers made us realized that our custom electrospinning devices needed to be improved. The focus here is on trying to fabricate scaffolds with satisfactory alignment of fibers and use them to validate our pSFDI device.

To validate our pSFDI device as an accurate way to study microstructures quickly and in a non-destructive way would significantly help the research considering that the sample being analyzed would still be intact and usable after being studied [12, 13].

Regarding the alignment of fibers, due to the inherent relationship between tissue's mechanical function and collagen fiber organization, being able to make scaffolds with satisfactory alignment is necessary in order to be able to use those scaffolds for applications such as tissue engineering, medicine, textile, etc. [4, 8, 21, 27].

This chapter summarizes the works pertaining to fabricating scaffolds with highly aligned electrospun fibers with our improved electrospinning process and validating our pSFDI device. Specifically, the studies include: (i) the fabrication of scaffolds with different thicknesses; (ii) the fabrication of scaffolds at different rotational speeds; and (iii) the validation of our pSFDI device. The remaining of this chapter is organized as follows. The procedures to make the electrospun scaffolds using the new auxiliary electrode and analyze them are described in Section 5.1. Section 5.2 presents the results of the different studies. The key findings and the implications of the aforementioned results are provided in Section 5.3.

5.1 Methods

5.1.1 Scaffolds Fabrication

All scaffolds were made following the Electrospinning Protocol given in **Appendix B**, using our custom electrospinning device.

As in Chapters 3 and 4, it was decided to make the scaffolds with Poly(ε-caprolactone) (PCL) and acetone as the biopolymer and non-toxic solvent, respectively. PCL 3 mm pellets with an average molecular weight of 80,000 g/mol (Sigma-Aldrich, USA) were dissolved in acetone (Sigma-Aldrich, USA).

For the study of the impact of electrospinning time, linked to the thickness of the scaffolds, it was decided to make them at the low speed this thesis research had started on, but with the other parameters chosen since then. Therefore, the scaffolds were made following the parameters shown in **Table 5-1**.

For the study on finding the optimal electrospinning speed, the scaffolds were made following the parameters shown in **Table 5-2**.

5.1.2 Use of the Cylindrical Auxiliary Electrode

The auxiliary electrode, consisting of an aluminum cylinder and its rubber sleeve (**Figure 5-1**), was slid onto the needle (**Figure 5-2**). The width of the cylinder was chosen such that the tip of the needle would poke out in order to enable its cleaning. As acetone is extremely volatile, at the tip of the needle, the polymer slowly solidifies thus sometimes obstructing it.

5.1.3 Thickness Measurement

Before mounting the sample onto the biaxial mechanical testing system, the thickness is measured using a non-contact laser displacement sensor (Keyence IL-030, USA). The sensor is placed on a flat surface and the tare of a 22x22 mm cover glass is calculated (**Figure 5-3**). The sample is then placed under the cover glass and pressure is applied with tweezers so that the true thickness of the sample can be measured.

5.2 Results

5.2.1 Results from the Investigation of the Visible Effects of the Cylinder

The cylinder had a significant impact on the electrospinning process. Indeed, the jet of fibers was now only collected on the mandrel and the size of the scaffold was significantly reduced (**Figure 5-4**). Moreover, over time, the thickness of the scaffolds made with the cylinder is greater than without the cylinder.

5.2.2 Results from the Thickness Study

For studying the effect of the electrospinning time, and thus the thickness of the scaffolds (**Table 5-3**), on fiber orientation, a trend was observed (**Figure 5-5**). Specifically, the fiber alignment is better for short electrospinning time. Also, the samples have more aligned fibers around θ_{fiber} = 25°–30°, where 0° and 180° are along the longitudinal axis. Indeed, almost all graphs have one predominant peak around the previously mentioned orientation. However, the more electrospinning time spent, the wider and/or smaller this peak becomes as well as shift position.

In addition to the predominant peak, every graph has another peak around 90° away from it. This will be discussed in **Section 5.3.3**.

5.2.3 Results from the Speed Study

Scaffolds were made at 1000, 2000, 3000, and 4000 rpm during an electrospinning time of 5 minutes and 10 minutes owing to the thickness study (**Section 5.3.2**) which demonstrated that a shorter electrospinning time would result in better fiber alignment. Unfortunately, pinpointing the best speed was not possible because all graphs show the same type of distribution (**Figure 5-6, Figure 5-7**).

However, it is noticed that the SEM distributions resemble the pSFDI distributions with the exception of a secondary peak. Specifically, in addition to the predominant peak, every pSFDI graph has another peak around a 90° offset from the dominant peak away from it. SEM imaging enabled us to consider that this secondary peak may be an aberration.

5.3 Discussion

5.3.1 Overall Findings from the Investigation on the Visible Effects of the Cylinder

This investigation showed the significant impact that the cylinder had on the electrospinning process. Indeed, what was thought to be normal, that is to say, fibers also collected in the vicinity of the mandrel, was very much not so. With the cylinder, the process was cleaner and thus more effective, i.e., with the jet now focused on the collector, the alignment of the fibers is improved.

5.3.2 Overall Findings from the Thickness Study

The present study mainly highlights the fact that the amount of fibers on the collector, related to the electrospinning time, is in direct relation to the fiber deposition and more importantly, the fiber alignment. Indeed, the more fibers are deposited on the collector, the less it attracts the

incoming fibers. It may even repel them, as the deposited fibers may retain some of their charges [14].

Moreover, the real orientation of the fibers seems to be θ_{fiber} = 25°–30°, where 0° and 180° are along the longitudinal axis. This goes against what seems logical and what can be read in the literature. Indeed, the fibers are supposed to be drawn by the collector around it, therefore aligned circumferentially [16, 20, 29, 34].

5.3.3 Overall Findings from the Speed Study

The expected findings from this study have unfortunately not been achieved. Specifically, pinpointing the optimal rotational speed of the collector with our current custom electrospinning device remains impossible. Future research should focus on finding the evaporation rate of the solvent so that the linear rate of the rotating mandrel matches it and enables fibers to be taken up on the surface of the collector [34].

However, this study has successfully provided insights on the pSFDI verification. The results show that similar distributions of fibers were obtained using scanning electron microscopy, which is a slow and destructive imaging method, and using pSFDI, which is on the contrary, a fast and non-destructive fiber imaging method to study microstructures using reflectance geometry [12, 13].

Nevertheless, pSFDI gives us a field of view that is much wider than the one from the SEM with which a specific spot is studied. Indeed, even the lowest magnitude does not allow us to view the whole sample. As a matter of fact, some SEM images can show very aligned fibers whereas at some other spots of the same scaffold, the fibers are not aligned the same way. Therefore, this is a limitation to take into account.

5.4 Concluding Remarks

In this chapter, one of the main objectives was to be able to make scaffolds with the most aligned fibers as possible. When acceptable results were obtained, the second main objective was to validate the use of our pSFDI device as a rapid and non-destructive method of study for microstructures. The first objective has only been partially reached, given that we were able to fabricate scaffolds with an acceptable fiber alignment distribution, but the fibers were not aligned in the expected direction. For the second objective, a successful outcome has been obtained but limitations have to be further studied to systematically validate the method.

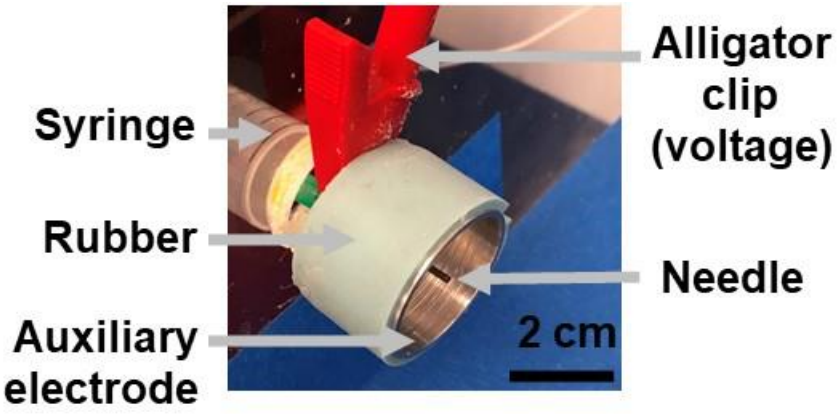

Figure 5-1. Photo of the auxiliary electrode on the needle.

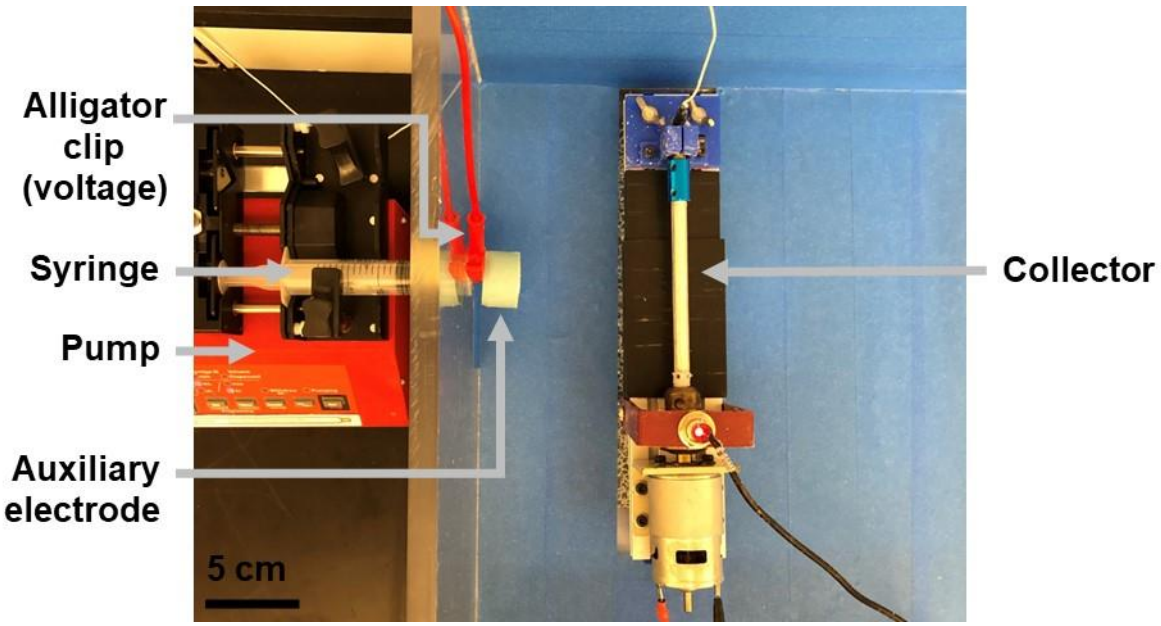

Figure 5-2. Photo, taken with a larger view, of the auxiliary electrode on the needle.

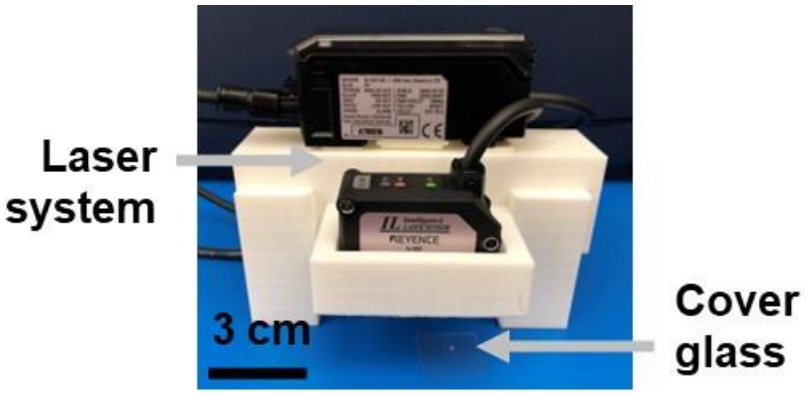

Figure 5-3. Photo of the laser system.

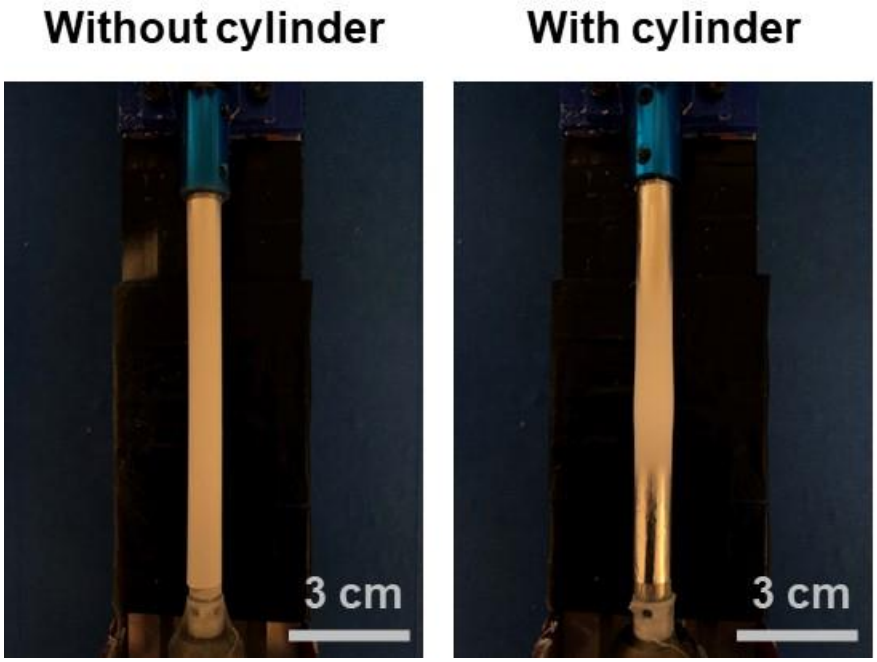

Figure 5-4. Photos of a scaffold made without the cylinder (*left*) and with the cylinder (*right*).

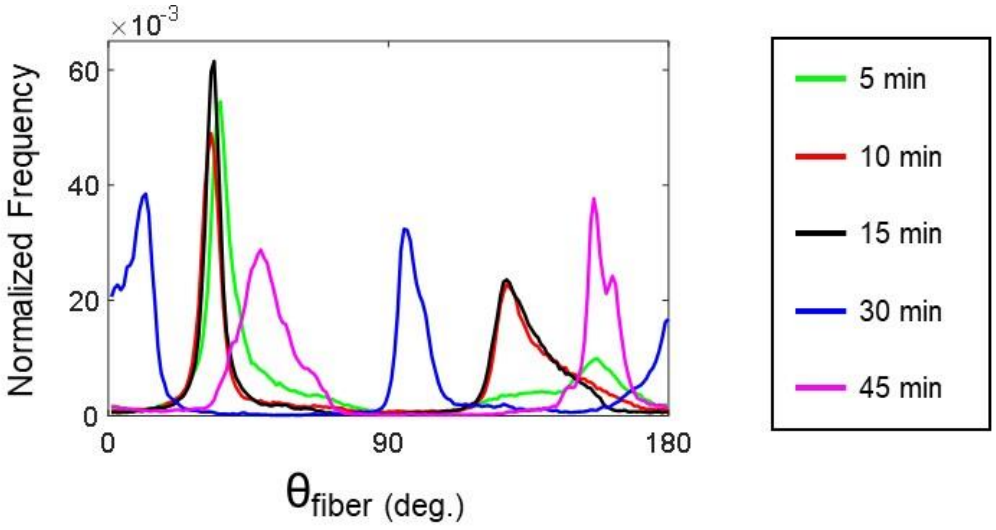

Figure 5-5. Fiber distributions with varying electrospinning times.

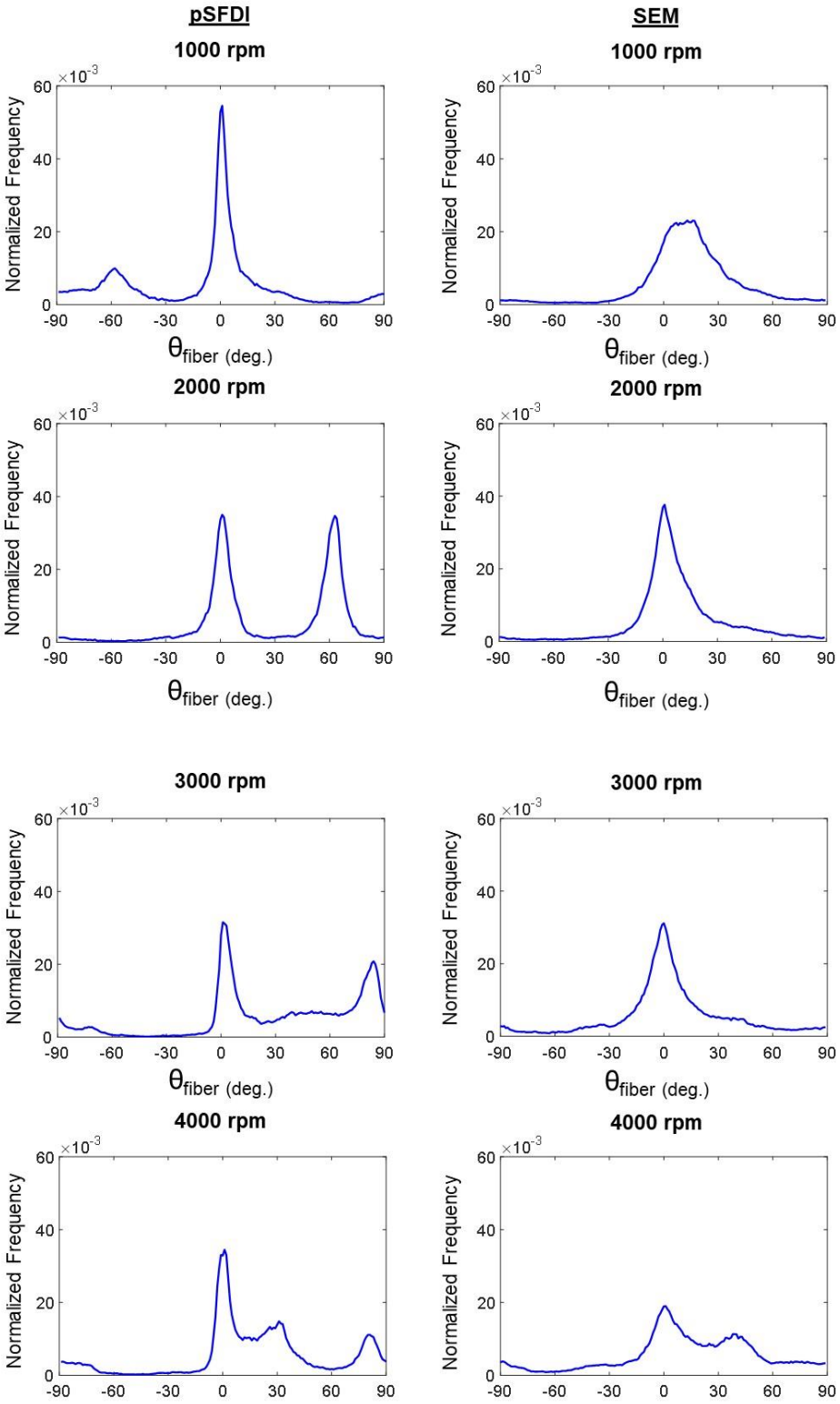

Figure 5-6. Fiber distributions at 5 min with various speeds for pSFDI (*left*) and SEM (*right*).

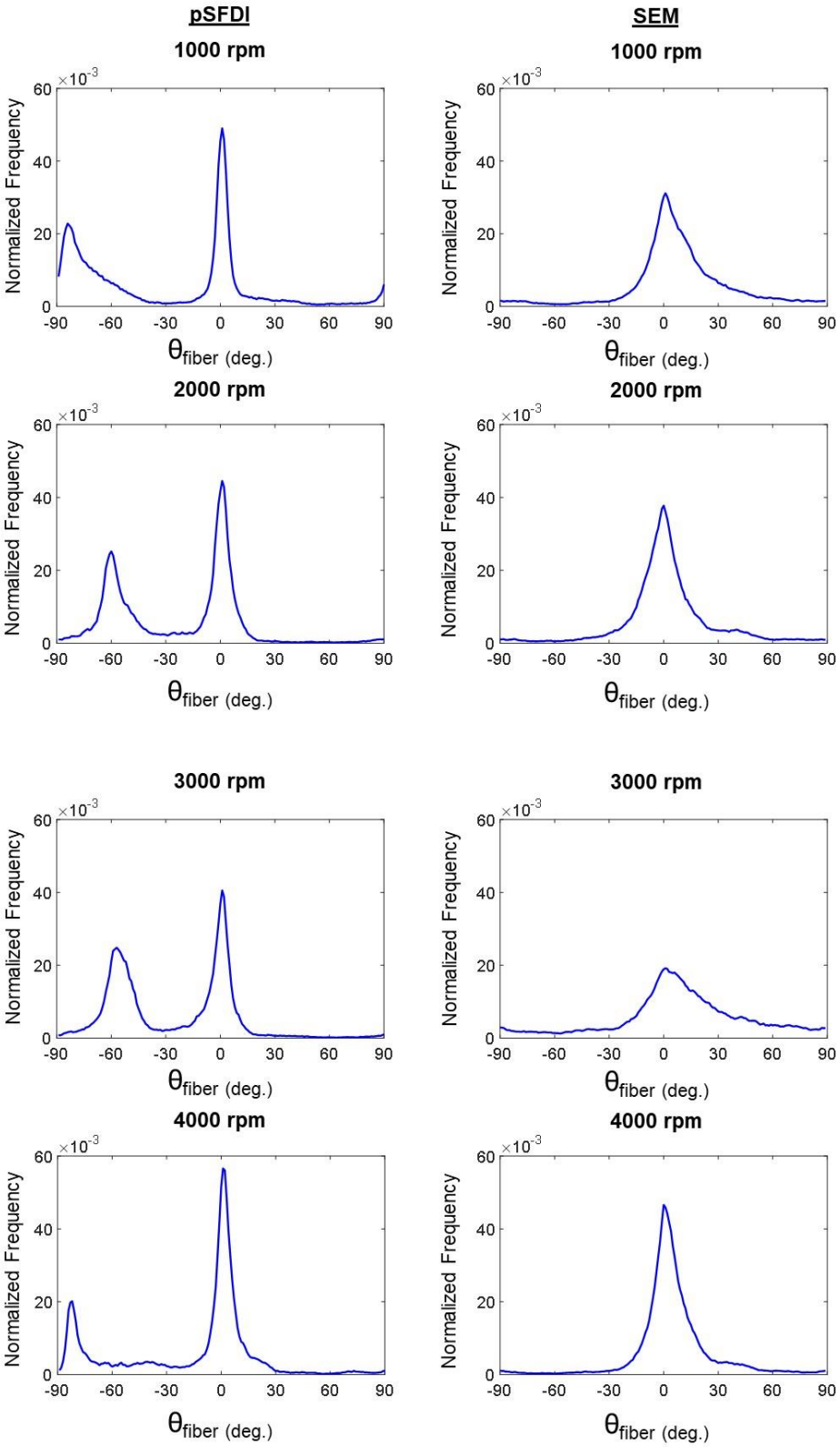

Figure 5-7. Fiber distributions at 10 min with various speeds analyzed by pSFDI (*left*) and SEM (*right*).

Table 5-1. Parameters for the fabrication of scaffolds to study fiber alignment with varying electrospinning time.

Experiment Tag	Concentration (%w/v)	TCD (cm)	Voltage (kV)	Flow Rate (mL/h)	Electrospinning Time (min)	Speed (rpm)
C5	15	10	20	5	5	1000
C10	15	10	20	5	10	1000
C15	15	10	20	5	15	1000
C30	15	10	20	5	30	1000
C45	15	10	20	5	45	1000

Table 5-2. Parameters for the fabrication of scaffolds to study fiber alignment with varying rotational speed.

Experiment Tag	Concentration (%w/v)	TCD (cm)	Voltage (kV)	Flow Rate (mL/h)	Electrospinning Time (min)	Speed (rpm)
C2005	15	10	20	5	**5**	2000
C2010	15	10	20	5	**10**	2000
C3005	15	10	20	5	**5**	3000
C3010	15	10	20	5	**10**	3000
C4005	15	10	20	5	**5**	4000
C4010	15	10	20	5	**10**	4000

Table 5-3. Thicknesses with varying electrospinning time.

Experiment Tag	Electrospinning Time (min)	Thickness (mm)
C5	5	0.11
C10	10	0.21
C15	15	0.25
C30	30	0.45
C45	45	0.46

CHAPTER 6 – CONCLUSIONS AND FUTURE WORK

6.1 Conclusions

Biodegradable polymer scaffolds can be used in very wide range of application such as medicine, textile, and filtration. Because electrospun scaffolds resemble extracellular matrix of biological systems such as collagen fibers, their use in tissue engineering is often studied. Experiments were done to advance the knowledge in the fabrication of satisfactory electrospun scaffolds with fibers whose diameters and orientation are controlled.

Studies showed that a decrease in concentration, an increase in distance tip-collector, and an increase in flow rate all reduce the fiber diameter, while an increase in concentration and flow rate help their alignment. However, the lack of reproducibility of the results made us realize that our custom device needed some further improvements. The use of an auxiliary electrode made it possible for the fabrication of scaffolds with more aligned fibers which were essential for the validation of our pSFDI device as a rapid and non-destructive technique to evaluate the microstructure of the synthesized scaffolds.

6.2 Recommendations for Future Research

This thesis concludes with recommendations for future work.

Regarding the electrospinning process, two of the frequently overlooked parameters are the humidity and temperature [6]. Knowing that the laboratory, in which the device is located, is kept at a low temperature with air conditioning, it may be needed to investigate how much the formation of fibers with the chosen polymer solution is influenced by these environmental

conditions. Finding the right temperature and humidity could significantly improve the reproducibility.

In addition, to avoid undesired deposition, the Tip-Collector Distance had been set at 10 cm before the implementation of the auxiliary electrode. With the cylinder now focusing the jet primarily on the collector, this parameter might need to be re-evaluated and quite possibly a greater distance can yield better and more reproducible results.

Furthermore, the linear rate of the revolving collector should theoretically match the evaporation rate of the solvent, such that the fibers are deposited and taken up on the mandrel's surface. Randomly oriented fibers are generated on the collector at the rotational rates slower than the fiber take-up speed so identifying the optimal speed with regard to the evaporation rate of acetone can be warranted as part of the future extensions [34].

Finally, computational modeling of the electrospinning process could be done prior to the realization of the experiments. If good models are found, this would reduce the time spent on trial and error by a lot and thus allow the researchers to advance in their work more efficiently.

Regarding the pSFDI device, during the analysis, the sample is bathed in a solution to mimic the analysis done for native soft tissues. However, the obtained results might be different if the scaffolds are kept in a dry condition that would require further investigations. Also, we are not quantifying the diffraction of light, so investigating it whether the sample is dry or wet could be of interest.

In addition, the samples are cut from the scaffolds and placed manually on the BioTester before being analyzed with the pSFDI: hence, the longitudinal axis of the scaffold may not be exactly placed at a zero-degree angle before analysis. Thus, the fiber orientation found during this

thesis research may not be the actual orientation of the fibers in the scaffolds. A way to quantify the angle at which the scaffold is analyzed is needed so that the accurate fiber orientation could be found in future investigations.

Finally, as mentioned in **Section 5.2.2**, within some of the pSFDI data, a secondary peak was observed that was not present in the SEM images. This can be due to two reasons:

(1) Difference in fields of view and depths

Even at the lowest magnitude, the SEM images only a portion of the sample analyzed completely with pSFDI. Thus, pSFDI might analyze fibers that we are not looking at with the SEM, areas where the fibers might not be as well aligned. A way to counteract that is to use the newer software with SEM, allowing you to stitch multiple images together to expand the field of view. Also, depending on the spatial frequency used, pSFDI analyses the sample more or less in depth, whereas SEM only images the surface of the sample.

(2) Misprediction made by the pSFDI

Due to the birefringent behavior of the fibers, there is a bimodal intensity response to the incident light going through the polarizer rotation from 0° to 180°. Therefore, the pSFDI can assimilate it as a secondary peak. More information on the theory of birefringent collagen scattering in *Jett et al.* [21]. Resolving this error would enable the creation of accurate graphs showing only the real fiber distribution.

APPENDIX A – NOMENCLATURE

Table A-1. Description of the abbreviations used throughout the thesis.

Category	Abbreviation	Description
Electrospinning	*d*	Diameter of the cylinder
	l	Length of the cylinder
	PBS	Phosphate-Buffered Saline
	PCL	Poly(ε-caprolactone)
	PEO	Poly(ethylene oxide)
	r	Radius of the cylinder
	rpm	Rotations per minute
	t	Thickness of the cylinder
	TCD	Tip-Collector Distance
Imaging	CCD	Charged-Coupled Device
	DLP	Digital Light Processing
	ESEM	Environmental Scanning Electron Microscopy
	LED	Light-Emitting Diode
	PLI	Polarized Light Imaging
	pSFDI	Polarized Spatial Frequency Domain Imaging
	SEM	Scanning Electron Microscopy
	SFDI	Spatial Frequency Domain Imaging
Analysis	*n*	Sample size
	SD	Standard Deviation
	θ_{fiber}	Fiber orientation
	$\theta_{polarizer}$	Polarizer transmission angle
Miscellaneous	AME	Aerospace and Mechanical Engineering
	BBDL	Biomechanics and Biomaterials Design Laboratory

APPENDIX B – ELECTROSPINNING PROTOCOL

In this appendix, the procedures to make the polymer solution, prepare the electrospinning device, and make the electrospun scaffold are presented.

Biomaterials and Biomechanics Design Laboratory

SRTC 2150

Electrospinning Protocol

Last revision: June 24, 2022

Materials

- Chemicals:
  - Polymer: polycaprolactone (PCL), polyethylene oxide (PEO)
  - Solvent: acetone, formic acid
- Glassware:
  - Beaker (2)
  - Airtight vial glass (1)
  - Watch glass (1)
  - Magnetic stirrer (1)
  - Syringe (1)
  - Pipette (1)
  - Pipette controller (1)
  - Spatula (1)
- Equipment:
  - Hotplate with magnetic stirrer.
  - Electrospinning device.
  - Balance. (Analytical if using polyethylene oxide).

Polymer Dilution

Safety: Wear gloves, goggles and a whitecoat for safety.

1. Weight polymer in a watch glass (**Figure B-1**). The amount of polymer will depend on the concentration of the solution (concentrations are typically reported as %w/v).
2. Under the fume hood, pipette the designated volume of solvent into an airtight glass vial.
3. Place vial on the hot plate. Turn the magnetic stirrer dial up slowly and set hotplate temperature to 80°C. Ideally a cone should form in the spinning solution.
4. Add polymer in small quantities with a spatula: PCL and PEO come in pellets so pour only 4 to 6 pellets at a time. Polymer might get attached to the edges of the vial; if this happens,

shift position of the beaker so the magnetic bar is able to move masses of accumulated polymer.

5. Ensure that the polymer is completely dissolved before proceeding.

Electrospinning Preparation (Figure B-3)

Safety: Wear gloves, goggles, and a white coat for safety.

1. Set Up the Collector.
    a. Cut a piece of aluminum to wrap around the collector.
    b. Make sure the aluminum is smooth, without wrinkles.
    c. Wrap the aluminum foil around the collector, shiny side up, and secure with glue.
    d. Place the collector into the electrospinning box.

2. Set up the Syringe.
    a. Connect an 18G needle to the syringe
    b. Pour the polymer solution into the syringe. Verify for clogs, check polymer flows smoothly into the syringe. When full, point syringe upwards and press slowly to remove bubbles.
    c. Place the syringe on the syringe pump.
    d. Secure syringe using the screws at the different points where the syringe is held by the pump.
    e. Move the pump to fit through the hole of the electrospinning box until the needle is completely inside of the box.
    f. Turn on the pump and enter in the parameters: the diameter of the syringe, the volume in the syringe, and the flow rate (mL/h).
    g. Start pumping and ensure that the liquid flows smoothly then stop pumping.

3. Set distance from tip of syringe to collector at the specified collection distance.
4. Prepare syringe with a small drop in the tip of the needle.
5. Connect voltage source (must be **OFF**) to the needle.
6. Check the collector's connection to ground. If loose, tighten bolt.
7. Connect the wires to the collector's motor.
8. Start collector making sure that it is spinning away from syringe. Use the tachometer to set the collector to the designated rpm.

Safety: From this point wear **Class III Safety Gloves** to operate <u>all</u> parts of the device.

9. Start pumping. Make sure polymer drops are forming at the tip of the needle.
10. Check voltage connection to needle. If plugged, turn on voltage source.
11. Voltage is set up to 20 kV by default. If needed to change, ramp up/down slowly.
12. Polymer jet should be formed at this point.

13. Check for polymer accumulation at unwanted parts (anything that is not the mandrel). If aluminum foil does not change to a whitish color in less than a min, polymer is accumulating somewhere else. Make sure to cover all metallic parts with paper towels or electric tape, if necessary.
14. If no accumulation is observed, syringe might be clogged, or pump is not set properly. Check that the black block that pushes the syringe is engaged.
15. When a buildup of polymer is on the tip of the syringe, wipe off using paper towels, **while wearing Class III Safety gloves**.
16. Keep overseeing the process, the syringe does not stop automatically.
17. If spinning needs to be stopped, paused, or finished:
    a. Turn off the voltage source.
    b. Stop the pump.
    c. Stop the collector.

Finalizing

1. Remove synthesized construct. Keep in a clean container/bag/surface. Label the bag with the date and electrospinning parameters.
2. Clean parts of the electrospinning apparatus. Take notes of where polymer built up, besides from the collector.
3. Turn off the devices and unplug them from the electrical outlet.
4. Dispose chemicals as per safety guidelines.

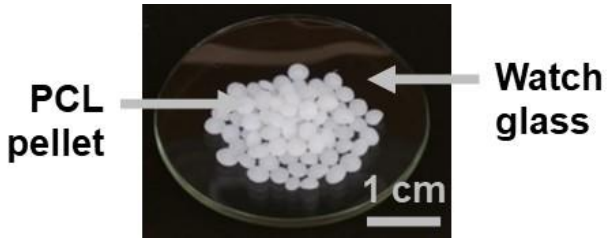

Figure B-1. Photo of PCL pellets.

Figure B-2. Photo of a vial on the magnetic hot plate.

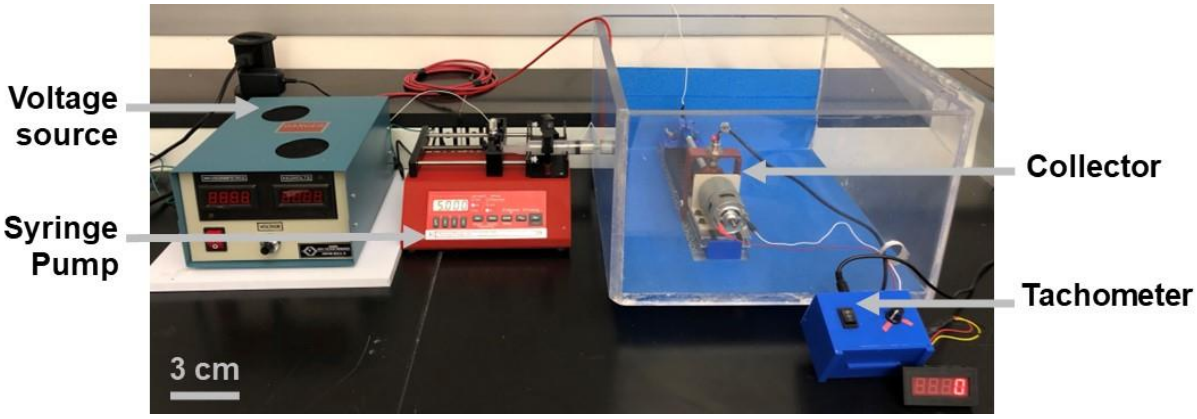

Figure B-3. Photo of the electrospinning setup.

APPENDIX C – DETAILED PSFDI TESTING PROCEDURES

In Appendix C, the detailed procedure for the pSFDI resulting in the imaging of the scaffolds is described.

The pSFDI is operated via Visual Studio (Microsoft Visual Studio, Microsoft, USA) in which a code programmed in Python (Python Software Foundation, USA) is used to image the samples. Once the sample is mounted onto the biaxial mechanical testing system (BioTester, CellScale Biomaterials Testing, Canada) as seen in **Section 3.1.2** and all the components of the pSFDI device are turned on, the code needs to be compiled. This will display a window where the test name for the imaging will be asked. Once the name has been given and a dedicated folder has been created, the Digital Light Processing (DLP) projection has to be set up. We have to choose a spatial frequency of 12 and a number of phases of 2 (this will result in the imaging of three phases named 0,1, and 2) to project the right pattern. Then the real time feed can be seen to adjust the brightness so that the image is not too bright or too dark, thus resulting in a poor quantification of the alignment of fibers. Finally, the setting to realize the AC Imaging has to be chosen as well. An index of 12 have to be selected to realize AC imaging, If DC imaging was required, another index would have to be chosen. Once the imaging is done, all the data can be found in a folder under the test name.

REFERENCES

1. Xue, J., Wu, T., Dai, Y., and Xia, Y., "Electrospinning and electrospun nanofibers: Methods, materials, and applications". *Chemical Reviews*, 2019. 119(8): pp. 5298-5415.
2. Santillán-Mercado, J.A., Rodríguez-Avilés, Y.G., Bello, S.A., González-Feliciano, J.A., and Nicolau, E., *Electrospun cellulose and nanocellulose composites as a biomaterial*, in *Electrospun biomaterials and related technologies*, J. Almodovar, Editor. 2017, Springer International Publishing: Cham. pp. 57-107.
3. Amna, R., Ali, K., Malik, M.I., and Shamsah, S.I., "A brief review of electrospinning of polymer nanofibers: History and main applications". *Journal of New Materials for Electrochemical Systems*, 2020. 23(3): pp. 151-163.
4. Mirjalili, M. and Zohoori, S., "Review for application of electrospinning and electrospun nanofibers technology in textile industry". *Journal of Nanostructure in Chemistry*, 2016. 6(3): pp. 207-213.
5. Shinoka, T., "Tissue engineered heart valves: Autologous cell seeding on biodegradable polymer scaffold". *Artificial Organs*, 2002. 26(5): pp. 402-406.
6. Ghobeira, R., Asadian, M., Vercruysse, C., Declercq, H., De Geyter, N., and Morent, R., "Wide-ranging diameter scale of random and highly aligned pcl fibers electrospun using controlled working parameters". *Polymer*, 2018. 157: pp. 19-31.
7. Kim, J.I., Hwang, T.I., Aguilar, L.E., Park, C.H., and Kim, C.S., "A controlled design of aligned and random nanofibers for 3D bi-functionalized nerve conduits fabricated via a novel electrospinning set-up". *Scientific Reports*, 2016. 6(1): p. 23761.
8. Amoroso, N., D'Amore, A., Hong, Y., Rivera, C., Sacks, M., and Wagner, W., "Microstructural manipulation of electrospun scaffolds for specific bending stiffness for heart valve tissue engineering". *Acta Biomaterialia*, 2012. 8(12): pp. 4268-4277.
9. Putti, M., Simonet, M., Solberg, R., and Peters, G.W.M., "Electrospinning poly(ε-caprolactone) under controlled environmental conditions: Influence on fiber morphology and orientation". *Polymer*, 2015. 63: pp. 189-195.
10. Yoo, H.S., Kim, T.G., and Park, T.G., "Surface-functionalized electrospun nanofibers for tissue engineering and drug delivery". *Advanced Drug Delivery Reviews*, 2009. 61(12): pp. 1033-1042.
11. Li, X., Huang, L., Li, L., Tang, Y., Liu, Q., Xie, H., Tian, J., Zhou, S., and Tang, G., "Biomimetic dual-oriented/bilayered electrospun scaffold for vascular tissue engineering". *Journal of Biomaterials Science, Polymer Edition*, 2020. 31(4): pp. 439-455.
12. Goth, W., Potter, S., Allen, A.C.B., Zoldan, J., Sacks, M.S., and Tunnell, J.W., "Non-destructive reflectance mapping of collagen fiber alignment in heart valve leaflets". *Annals of Biomedical Engineering*, 2019. 47(5): pp. 1250-1264.
13. Yang, B., Lesicko, J., Sharma, M., Hill, M., Sacks, M.S., and Tunnell, J.W., "Polarized light spatial frequency domain imaging for non-destructive quantification of soft tissue fibrous structures". *Biomedical Optics Express*, 2015. 6(4): pp. 1520-1533.

14. Stanger, J., Tucker, N., Wallace, A., Larsen, N., Staiger, M., and Reeves, R., "The effect of electrode configuration and substrate material on the mass deposition rate of electrospinning". *Journal of Applied Polymer Science*, 2009. 112(3): pp. 1729-1737.

15. Yang, Y., Jia, Z., Liu, J., Li, Q., Hou, L., Wang, L., and Guan, Z., "Effect of electric field distribution uniformity on electrospinning". *Journal of Applied Physics*, 2008. 103(10): p. 104307.

16. Robinson, A.J., Pérez-Nava, A., Ali, S.C., González-Campos, J.B., Holloway, J.L., and Cosgriff-Hernandez, E.M., "Comparative analysis of fiber alignment methods in electrospinning". *Matter*, 2021. 4(3): pp. 821-844.

17. Doshi, J. and Reneker, D.H., "Electrospinning process and applications of electrospun fibers". *Journal of Electrostatics*, 1995. 35(2): pp. 151-160.

18. Goldstein, J.I., Newbury, D.E., Michael, J.R., Ritchie, N.W., Scott, J.H.J., and Joy, D.C., "*Scanning Electron Microscopy and X-ray Microanalysis"*. 2017: Springer.

19. Chronakis, I.S., "Novel nanocomposites and nanoceramics based on polymer nanofibers using electrospinning process—a review". *Journal of Materials Processing Technology*, 2005. 167(2-3): pp. 283-293.

20. Long, Y.-Z., Yan, X., Wang, X.-X., Zhang, J., and Yu, M., *Chapter 2 - Electrospinning: The setup and procedure*, in *Electrospinning: Nanofabrication and applications*, B. Ding, X. Wang, and J. Yu, Editors. 2019, William Andrew Publishing. pp. 21-52.

21. Jett, S.V., Hudson, L.T., Baumwart, R., Bohnstedt, B.N., Mir, A., Burkhart, H.M., Holzapfel, G.A., Wu, Y., and Lee, C.-H., "Integration of polarized spatial frequency domain imaging (pSFDI) with a biaxial mechanical testing system for quantification of load-dependent collagen architecture in soft collagenous tissues". *Acta Biomaterialia*, 2020. 102: pp. 149-168.

22. Bosworth, L.A. and Downes, S., "Acetone, a sustainable solvent for electrospinning poly(ε-caprolactone) fibres: Effect of varying parameters and solution concentrations on fibre diameter". *Journal of Polymers and the Environment*, 2012. 20(3): pp. 879-886.

23. Rabionet, M., Yeste, M., Puig, T., and Ciurana, J., "Electrospinning PCL scaffolds manufacture for three-dimensional breast cancer cell culture". *Polymers*, 2017. 9(8): p. 328.

24. Yuan, H., Zhao, S., Tu, H., Li, B., Li, Q., Feng, B., Peng, H., and Zhang, Y., "Stable jet electrospinning for easy fabrication of aligned ultrafine fibers". *Journal of Materials Chemistry*, 2012. 22(37): pp. 19634-19638.

25. Schervish, M.J., "P values: What they are and what they are not". *The American Statistician*, 1996. 50(3): pp. 203-206.

26. Van der Schueren, L., De Schoenmaker, B., Kalaoglu, Ö.I., and De Clerck, K., "An alternative solvent system for the steady state electrospinning of polycaprolactone". *European Polymer Journal*, 2011. 47(6): pp. 1256-1263.

27. Kim, G.H. and Yoon, H., "Effect of an auxiliary electrode on the crystalline morphology of electrospun nanofibers". *Applied Physics Letters*, 2008. 93(2): p. 023127.

28. Kim, G.H., “Electrospun PCL nanofibers with anisotropic mechanical properties as a biomedical scaffold”. *Biomedical Materials,* 2008. 3(2): p. 025010.

29. Becker, A., Zernetsch, H., Mueller, M., and Glasmacher, B., “A novel coaxial nozzle for in-process adjustment of electrospun scaffolds’ fiber diameter: Electrospun mats and their dependence on process parameters”. *Current Directions in Biomedical Engineering*, 2015. 1(1): pp. 104-107.

30. Kim, G., Cho, Y.-S., and Kim, W.D., “Stability analysis for multi-jets electrospinning process modified with a cylindrical electrode”. *European Polymer Journal,* 2006. 42(9): pp. 2031-2038.

31. Kim, G. and Kim, W., “Nanofiber spraying method using a supplementary electrode”. *Applied Physics Letters,* 2006. 89(1): p. 013111.

32. Kim, G.H., “Electrospinning process using field-controllable electrodes”. *Journal of Polymer Science Part B: Polymer Physics,* 2006. 44(10): pp. 1426-1433.

33. Kim, G. and Kim, W., “Highly porous 3D nanofiber scaffold using an electrospinning technique”. *Journal of Biomedical Materials Research Part B: Applied Biomaterials: ,* 2007. 81(1): pp. 104-110.

34. Baji, A., Mai, Y.-W., Wong, S.-C., Abtahi, M., and Chen, P., “Electrospinning of polymer nanofibers: Effects on oriented morphology, structures and tensile properties”. *Composites Science and Technology*, 2010. 70(5): pp. 703-718.

35. Suresh, S., Becker, A., and Glasmacher, B., “Impact of apparatus orientation and gravity in electrospinning - A review of empirical evidence”. *Polymers*, 2020. 12(11): p. 2448.

36. Hudson, L,T., Laurence, D.W., Lau, H.M., Mullins, B.T., Doan, D.D., and Lee, C.-H., “Linking collagen fiber architecture to tissue-level biaxial mechanical behaviors of porcine semilunar heart valve cusps”. *Journal of the Mechanical Behavior of Biomedical Materials,* 2022. 125(1): p. 104907.